Micro Flapping-Wing Vehicles Formation Control With Attitude Estimation

Wanyue Jiang, Dongyu Li, *Member, IEEE*, and Shuzhi Sam Ge, *Fellow, IEEE*

***Abstract*—This article addresses the formation control problem of flapping-wing vehicles (FWVs) under the model uncertainty and the measurement inaccuracy. A two-layer formation strategy is adopted, which consists of a formation control layer for the leaders, and a containment control layer for the followers. In both layers, attitudes and positions are required by the formation geometry. A formation state estimation algorithm is designed to achieve the desired formation states from local neighborhoods. In FWVs, attitude angles are usually achieved from angular velocities, whose measurement error accumulates during integration and leads to divergence of the system. In order to solve this problem, we explore the coupling property between the translational motion and the rotational motion of FWVs, and design a coupling-based estimation method for attitude angles. To compensate for the model uncertainty, the measurement error, and the estimation error, adaptive neural networks are developed together with the control algorithm. The stability of both the control algorithm and the estimation algorithm is guaranteed based on the Lyapunov stability theory. Simulations are conducted to validate our method, and the results illustrate its effectiveness.**

***Index Terms*—Euler–Lagrange systems, Formation control, neural networks (NNs), micro flapping-wing vehicle (FWV).**

I. Introduction

INSPIRED by the characteristics of insects and birds, flapping-wing vehicles (FWVs) are developed by researchers [1]. Compared with fixed-wing aerial vehicles and the rotorcraft, the flapping-wing structure is more fitted to the micro aircraft. FWVs combine the advantages of the two previous categories, such as high-speed forward flight, hovering, vertical take-off and landing, and good maneuverability. Moreover, they can naturally conceal themselves or pretend to be an insect to conduct special tasks.

As early as 1993, the mechanism of the FWV is studied [2] and its aerodynamic model is constructed [3]. The dynamics and control mechanism are further investigated by many researchers [4], [5]. In 2011, a Nano Hummingbird is built by the Aero Vironment team after over four years of work [6]. An attitude and the position control method for this flapping-wing model is designed on the basis of the adaptive sliding-mode technique [7]. The model uncertainty is considered and an adaptive neural-network (NN) method is adopted to control the FWV [8]. Disturbance rejection schemes of FWVs are also explored for the outdoor wind condition [9]. The manual control and autonomous flight can be achieved by these methods; however, they are designed for a single FWV. The cooperation of multiple FWVs can be more advantageous for complicated tasks.

The formation problem is one of the most fundamental and important tasks for multiagent cooperation. The generalized formation control is defined as driving multiple agents to achieve prescribed constraints on their states [10], [11], whereas the narrow formation control emphasizes on driving multiple agents to form the desired geometry pattern [12]. Despite work on formation geometry, there are also efforts made on the cooperative control of multiple agents. The consensus control aims to make the states of the agents reach a common value [13], [14], whereas the containment control requires that a team of followers be guided by multiple leaders [15], [16].

The rotorcraft, the fixed-wing aerial vehicle, and the spacecraft are three typical types of agents in the aerial formation control. In [17], the formation tracking problem is studied subjected to switching topologies with the application to the quadrotor, only translational motion is considered for the quadrotor, and it is modeled as a second-order system. In [18], a translational tracking control method for the spacecraft is designed to construct a formation. Despite the translational motion, the formation problem with respect to the rotational motion is also studied [19]–[21]. In some works, the translational motion and the rotational motion are regarded as a coupled system, for example, the formation control problem of fixed-wing aerial vehicles or ground vehicles [22]–[24]. They are always described as the so-called unicycle model, which actually have three degrees of freedom: 1) the forward velocity; 2) the pitch angle; and 3) the heading angle. The motion of the 2-D unicycle agent is always decomposed to the heading vector and its perpendicular vector [25]–[27], and the control input is linearly formulated by these intermediate vectors. The polar coordinate is also widely used for unicycle agents [28], [29]. In [30], both the translational motion and the rotational motion are controlled for the formation of quadrotors, and they are considered as decoupled motion and handled

Manuscript received October 4, 2019; revised March 29, 2020; accepted April 8, 2020. Date of publication May 28, 2020; date of current version February 16, 2022. This work was supported by the China Scholarship Council under Grant 201706830077. This article was recommended by Associate Editor Y. Pan. *(Corresponding author: Dongyu Li.)*

Wanyue Jiang is with the Institute for Future, Qingdao University, Qingdao 266071, China.

Dongyu Li is with the Department of Electrical and Computer Engineering, National University of Singapore, Singapore 117576, and also with the Department of Control Science and Engineering, Harbin Institute of Technology, Harbin 150001, China (e-mail: lidy@hit.edu.cn).

Shuzhi Sam Ge is with the Department of Electrical and Computer Engineering, National University of Singapore, Singapore 117576.

Color versions of one or more figures in this article are available at https://doi.org/10.1109/TCYB.2020.2988911.

Digital Object Identifier 10.1109/TCYB.2020.2988911

separately. In the formation control of the spacecraft, there are also works dealing with both the translational motion and the rotational motion, whereas the coupling between them is analyzed for decoupled control [31], [32]. Different from these works, we consider both the translational motion and the rotational motion in FWVs, and the coupling property between them is considered very helpful in this article.

Attitude angles of many small aircraft are achieved mediately from the integration of angular velocities [33], [34]. The measurement errors accumulate over time by integration and lead to drift in long-time flight. Usually, auxiliary sensors are adopted to solve this problem at the price of larger space and weight. In this article, both model uncertainties and measurement errors are considered during flight, an adaptive NNs-based control algorithm and a state estimation algorithm are designed for the formation control problem. The contributions of this article are as follows.

1) A two-layer formation control method combined with adaptive NNs and attitude estimation is proposed for the FWV formation under model uncertainties and measurement errors. Using the proposed method, both tracking errors and estimation errors will remain within small compact sets. In contrast, most of the existing works for multiple Euler–Lagrange systems deal with either known systems or parametric uncertainties with the linearity-in-parameters assumption [35], [36].
2) Both the translational motion control and the rotational motion control are considered in the formation, and the coupling property between them is analyzed. Defined as "coupled by coordinate transformation," the coupling property is considered as useful information in our scheme. In contrast, most existing works either consider the translational tracking control [18] and the rotational tracking control [19], [20] separately for the formation or analyze the coupling property for decoupling [31], [32].
3) Using the specific coupling property, an estimation algorithm for attitude angles is designed to prevent them from drifting away, which is caused by the measurement inaccuracy of angular velocities. In contrast, most of the state estimators consider only the output-feedback situation, and the outer loop information is needed for unmeasurable states [37]–[40].
4) A finite-time sliding-mode state estimator is designed to achieve the desired translational and rotational state information. Using the estimator, the control law proposed in this article is fully distributed, whereas global information is commonly required in the control level of formation problems [41], [42].

II. Problem Formulation and Preliminaries

A. Graph Theory

Graphs are commonly used to describe network topologies of multiagent systems. A graph $\mathcal{G} = (V, E)$ consists of two parts: 1) a vertex set V and 2) an edge set E. The size of V is determined by the number of agents. We have N leaders and M followers in the system, thus $V = [1, 2, \ldots, N + M]$. The edge set $E \subseteq V \times V$ describes the connection between vertices. $(i, j) \in E$ indicates that the agent j can achieve information from the agent i. The adjacency matrix $\mathcal{A} = [a_{ij}] \in \mathbb{R}^{(N+M)\times(N+M)}$ is the non-negative weight matrix of the edges. If $(i, j) \in E$, $a_{ij} > 0$; otherwise, $a_{ij} = 0$. The Laplacian matrix is defined as $\mathcal{L} = [l_{ij}]$, where $l_{ii} = \sum_{j\neq i} a_{ij}$ and $l_{ij} = -a_{ij}$ for $i \neq j$.

B. Agent Dynamics

The dynamics of the FWV is introduced [7]. The translational motion equation of the FWV is derived directly from aerodynamic forces. Using the mass matrix $M_{iT} = m_i I_{3\times 3}$ and the gravity vector $G_{iT} = [0, 0, -m_i g]^{\mathrm{T}}$, the Euler–Lagrange equation for the translational motion can be written as

$$M_{iT}\ddot{\boldsymbol{q}}_{iT} + G_{iT} = H_{IB}(\boldsymbol{q}_{iR})\boldsymbol{u}_{iT} \tag{1}$$

where $\boldsymbol{u}_{iT}$ is the translational motion control input, $\boldsymbol{q}_{iT} = [x_i, y_i, z_i]^{\mathrm{T}}$ is the translational state vector, subscript i represents the ith FWV, subscript T stands for the translational motion, and H_{IB} is the rotation matrix from the body frame to the inertial frame

$$\begin{aligned} H_{IB}(\boldsymbol{q}_{iR}) = &\begin{bmatrix} \cos\psi_i & -\sin\psi_i & 0 \\ \sin\psi_i & \cos\psi_i & 0 \\ 0 & 0 & 1 \end{bmatrix} \\ &\times \begin{bmatrix} \cos\theta_i & 0 & \sin\theta_i \\ 0 & 1 & 0 \\ -\sin\theta_i & 0 & \cos\theta_i \end{bmatrix} \\ &\times \begin{bmatrix} 1 & 0 & 0 \\ 0 & \cos\phi_i & -\sin\phi_i \\ 0 & \sin\phi_i & \cos\phi_i \end{bmatrix}. \end{aligned} \tag{2}$$

Remark 1: The rotation matrix H_{IB} is always invertible. Its inverse matrix H_{BI} is the rotation matrix from the inertial frame to the body frame. H_{BI} is also the transposed matrix of H_{IB}, namely, $H_{BI} = H_{IB}^{-1} = H_{IB}^{\mathrm{T}}$.

The rotational motion equation is calculated in the body frame

$$\begin{aligned} \dot{\boldsymbol{\eta}}_i &= \bar{I}_3\dot{\boldsymbol{w}}_i + \boldsymbol{w}_i \times \bar{I}_3\boldsymbol{w}_i \\ &= \bar{I}_3\frac{d}{dt}(H_i\dot{\boldsymbol{q}}_{iR}) + (H_i\dot{\boldsymbol{q}}_{iR}) \times \bar{I}_3(H_i\dot{\boldsymbol{q}}_{iR}) = \boldsymbol{u}_{iR} \end{aligned} \tag{3}$$

where $\boldsymbol{\eta}_i$ is the angular momentum, $\bar{I}_3$ is the moment of inertia matrix, $\boldsymbol{q}_{iR} = [\phi_i, \theta_i, \psi_i]^{\mathrm{T}}$ is the rotational state vector with ϕ the roll angle, θ the pitch angle, and ψ the yaw angle. Subscript R stands for the rotational motion. We use bars to distinguish the inertia matrix from the identity matrix. H_i is the transfer matrix from rotational velocities to translational velocities

$$H_i = \begin{bmatrix} 1 & 0 & -\sin\theta_i \\ 0 & \cos\phi_i & \cos\theta_i\sin\phi_i \\ 0 & -\sin\phi_i & \cos\theta_i\cos\phi_i \end{bmatrix}. \tag{4}$$

Using a square matrix L_i such that

$$(H_i\dot{\boldsymbol{q}}_{iR}) \times \bar{I}_3(H_i\dot{\boldsymbol{q}}_{iR}) = L_i\dot{\boldsymbol{q}}_{iR}. \tag{5}$$

Equation (3) can be written as

$$M_{iR}\ddot{\boldsymbol{q}}_{iR} + C_{iR}\dot{\boldsymbol{q}}_{iR} = \boldsymbol{u}_{iR} \tag{6}$$

where $M_{iR} = \bar{I}_3 H_i$ and $C_{iR} = \bar{I}_3\dot{H}_i + L_i$.

Bring the translational motion and the rotational motion together, the FWV can be modeled as an Euler–Lagrange system

$$M_i(\boldsymbol{q}_i)\ddot{\boldsymbol{q}}_i + C_i(\boldsymbol{q}_i, \dot{\boldsymbol{q}}_i)\dot{\boldsymbol{q}}_i + G_i = H(\boldsymbol{q}_i)\boldsymbol{u}_i \tag{7}$$

where $\boldsymbol{q}_i = [\boldsymbol{q}_{iT}^{\mathrm{T}}, \boldsymbol{q}_{iR}^{\mathrm{T}}]^{\mathrm{T}}$, $M_i(\boldsymbol{q}_i) \in \mathbb{R}^{6\times 6}$ is the symmetric positive-definite inertia matrix, $C_i(\boldsymbol{q}_i, \dot{\boldsymbol{q}}_i) \in \mathbb{R}^{6\times 6}$ is the matrix of Coriolis forces, G_i denotes the gravitational force, $\boldsymbol{u}_i$ is the control input vector, and $\boldsymbol{q}_i$ denotes the state vector of the ith FWV. The matrices and vectors in (7) are presented as follows:

$$M_i = \begin{bmatrix} M_{iT} & 0 \\ 0 & M_{iR} \end{bmatrix},\ C_i = \begin{bmatrix} 0 & 0 \\ 0 & C_{iR} \end{bmatrix},\ G_i = \begin{bmatrix} G_{iT} \\ 0 \end{bmatrix}$$
$$H(\boldsymbol{q}_i) = \begin{bmatrix} H_{IB}(\boldsymbol{q}_{iR}) & 0 \\ 0 & I_{3\times 3} \end{bmatrix},\ \boldsymbol{u}_i = \begin{bmatrix} \boldsymbol{u}_{iT} \\ \boldsymbol{u}_{iR} \end{bmatrix}. \tag{8}$$

Property 1 [43]: The matrix $\dot{M}_{iR} - 2C_{iR}$ is skew symmetric.

Remark 2: The translational control input $\boldsymbol{u}_{iT}$ is physically the aerodynamic force in the body frame, and the rotational control input $\boldsymbol{u}_{iR}$ is physically the aerodynamic torque in the body frame. The Euler–Lagrange formulation in (7) fits for a variety of aerial objects. Since the translational motion is more important in the inertial frame than in the body frame, $H_{IB}(\boldsymbol{q}_{iR})$ in (1) is used for coordinate transformation.

C. Problem Description and Coupling Analysis

Consider that the formation problem contains N leader FWVs labeled as $1, 2, \ldots, N$ and M follower FWVs labeled as $N+1, N+2, \ldots, N+M$. In the system, the Laplacian matrix $\mathcal{L} \in \mathbb{R}^{(N+M)\times(N+M)}$ can be written as

$$\mathcal{L} = \begin{bmatrix} \mathcal{L}_{L1} & 0_{N\times M} \\ \mathcal{L}_{F2} & \mathcal{L}_{F1} \end{bmatrix} \tag{9}$$

where $\mathcal{L}_{L1}$ is the network topology among the leaders, $\mathcal{L}_{F1}$ is the network topology among the followers, and $\mathcal{L}_{F2}$ is the network topology between the leaders and the followers. Let $\mathcal{L}_{L2} = [-a_{10}, -a_{20}, \ldots, -a_{N0}]^{\mathrm{T}}$ denote whether the leader can access the formation trajectory, where $a_{i0} = 1$ if yes, and $a_{i0} = 0$ otherwise. Denote $\mathcal{G}_l = (V_l, E_l)$ the communication network topology graph of the N leaders, with $V_l = [1, 2, \ldots, N]$ and $E_l = V_l \times V_l$. The adjacency matrix of the N leaders is

$$\mathcal{A}_l = \begin{bmatrix} a_{00} & \cdots & a_{0N} \\ \vdots & \ddots & \vdots \\ a_{N0} & \cdots & a_{NN} \end{bmatrix} \tag{10}$$

where a_{ij} is the non-negative weight of the edges in the graph.

Assumption 1 [44]: For the N leaders, $\mathcal{G}_l$ is connected. For the M followers, there exists at least one path from the leader set to each follower.

Lemma 1 [45]: Each entry of $-\mathcal{L}_{F1}^{-1}\mathcal{L}_{F2}, -\mathcal{L}_{L1}^{-1}, -\mathcal{L}_{L1}^{-1}\mathcal{L}_{L1}$ is negative and each row sum of $-\mathcal{L}_{F1}^{-1}\mathcal{L}_{F2}, -\mathcal{L}_{L1}^{-1}, -\mathcal{L}_{L1}^{-1}\mathcal{L}_{L1}$ is equal to one. $\mathcal{L}_{L1} \in \mathbb{R}^{N\times N}$ and $\mathcal{L}_{F1} \in \mathbb{R}^{M\times M}$ are symmetric positive definite.

Remark 3: Note that the concept of the leader in [45] is properly modified here for greater clarity. In this approach, a leader does not necessarily have no neighbors, but it does not have follower neighbors. Therefore, leaders do not get information from followers, whereas followers achieve information from leaders. Since the connectivity is the same in both systems, Lemma 1 works.

This article focuses on the two-layer formation control problem of FWVs, whose formation structure is similar as in [46]. In the first layer, leaders move together to achieve a specified formation with the desired reference. In the second layer, followers converge into the convex hull spanned by leaders. To construct a splendid formation, the configuration is required not only for the translational motion of the FWVs but also for their rotational motion.

We consider the formation control problem in which attitude angles cannot be achieved directly and angular velocities cannot be measured accurately. To address this problem, we design an estimation algorithm for attitude angles. Moreover, adaptive NNs are employed to compensate for model uncertainties.

Remark 4: In [46], different estimation and control methods are designed for constant and time-varying configurations. In this article, we use a unified method for both constant and time-varying configurations. Both the translational motion and the rotational motion are controlled for the desired configuration.

Remark 5: Attitude angles of the aircraft are commonly achieved from the integration of angular velocities, which are measured by gyroscopes. The measurement error accumulates over time and leads to drift in long-time flight. Usually, magnetometer and accelerometer are used as auxiliary sensors to prevent the drift of attitude angles. In micro FWVs, extra sensors cause larger space and weight.

Remark 6: Compared with output-feedback control methods in [37]–[40] which estimate unmeasurable states using output states, the estimation of attitude angles is much more challenging. The reason is that output states are the outer loop information for their unmeasurable states, whereas angular velocities which can be measured in our system are the inner loop information. Attitude angles cannot be estimated using only angular velocities due to the measurement inaccuracy, therefore, coupling information is explored to help.

In order to estimate attitude angles of the FWV without drift, the coupling information is used. In (7), the translational motion of the FWV is coupled with its rotational motion via a matrix $H_{IB}(\boldsymbol{q}_{iR})$, we call it "coupled by coordinate transform."

Definition 1: In an Euler–Lagrange system, the translational motion is said to be coupled by coordinate transform with the rotational motion if the translational control input has component generated directly in the body frame and the component has full rank.

The coupling concept has the following features.

1) The translational control input has components generated in the body frame. For the control of the translational motion in the motion frame (usually inertial frame), the coordinate transformation has to be conducted from the body frame to the motion frame. Rotational states are coupled during the coordinate transformation process.

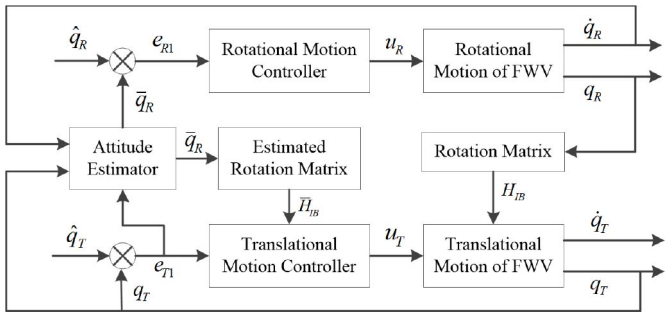

Fig. 1. Estimate attitude angles using coupling information.

2) The component of the translational control input in the body frame has full rank. The translational motion can be controlled by the translational control input with any rotational state.

In our case, the control input of the translational motion has the same rank with the translational states, and its coefficient matrix is invertible. Therefore, the translational motion is controllable.

The schematic is shown in Fig. 1. In the design of the translational motion control algorithm, estimated attitude angles are used instead of their real values. Since the estimation error leads to the tracking error in the translational motion, we can adjust the estimated attitude angles using translational information and prevent attitude angles from drifting away.

D. Useful Technical Lemmas and Definitions

Lemma 2: If there exist real numbers $c > 0$ and $\alpha \in (0, 1)$ such that a Lyapunov function V satisfies

$$\dot{V}(x) + c(V(x))^{\alpha} \leq 0 \tag{11}$$

the origin is a finite-time stable equilibrium for V with T the settling-time function

$$T(x) \leq \frac{1}{c(1-\alpha)} V(x)^{1-\alpha}. \tag{12}$$

Assumption 2: The measured angular velocity $\bar{\boldsymbol{v}}_R$ is in the neighborhood of its real value $\boldsymbol{v}_R$. Mathematically, there exists a positive constant $\epsilon_{\boldsymbol{v}}$ such that

$$\|\tilde{\boldsymbol{v}}_R\| \leq \epsilon_{\boldsymbol{v}} \tag{13}$$

where $\tilde{\boldsymbol{v}}_R = \boldsymbol{v}_R - \bar{\boldsymbol{v}}_R$, and $\boldsymbol{v}_R = \dot{\boldsymbol{q}}_R$.

III. Distributed Formation Control Method

A. Finite-Time Estimator for the Leaders

Inspired by [46], we use the following estimation algorithm for the formation states of the leaders:

$$\begin{aligned} \dot{\hat{\boldsymbol{q}}}_i &= \hat{\boldsymbol{v}}_i - \beta_1 \mathrm{sgn} \sum_{j=0}^{N} a_{ij}\big(\hat{\boldsymbol{q}}_i - \hat{\boldsymbol{q}}_j - \boldsymbol{\delta}_{ij}\big) \\ \dot{\hat{\boldsymbol{v}}}_i &= -\beta_2 \mathrm{sgn} \sum_{j=0}^{N} a_{ij}\big(\hat{\boldsymbol{v}}_i - \hat{\boldsymbol{v}}_j - \dot{\boldsymbol{\delta}}_{ij}\big) \end{aligned} \tag{14}$$

where β_1 and β_2 are positive parameters with respect to the convergence rate of the formation state estimation process, $\hat{\boldsymbol{q}}_i$ and $\hat{\boldsymbol{v}}_i$, $i = 1, 2, \ldots, N$, are the desired formation positions and velocities for the translational motion, and the desired attitude angles and angular velocities for the rotational motion, distinguished by subscripts T and R. Denote $\boldsymbol{\delta}_{ij} = \boldsymbol{\delta}_i - \boldsymbol{\delta}_j$ the desired relative distance between FWV i and FWV j, with $\boldsymbol{\delta}_i$ and $\boldsymbol{\delta}_j$ the desired trajectory of them. $\boldsymbol{\delta}_{i0}$ represents the relative distance between FWV i and the desired trajectory of the formation. Initially, $\hat{\boldsymbol{q}}_0 = \boldsymbol{q}_0 = \boldsymbol{\delta}_0$ and $\hat{\boldsymbol{v}}_0 = \dot{\boldsymbol{q}}_0 = \dot{\boldsymbol{\delta}}_0$. Subscript 0 stands for the formation trajectory information, and subscripts T and R are ignored because the algorithm in (14) fits for both translational and rotational motions.

The operation of the function sgn is [47]

$$\mathrm{sgn}(\boldsymbol{x}) \triangleq \frac{\boldsymbol{x}}{\|\boldsymbol{x}\|}, \boldsymbol{x} \neq 0. \tag{15}$$

The function defines a unit vector in the direction of $\boldsymbol{x}$. It covers an n-dimensional unit ball.

Remark 7: $\boldsymbol{\delta}_{ij}$ controls the shape of the formation. In our scheme, $\boldsymbol{\delta}_{ij}$ is known instead of $\boldsymbol{\delta}_i$ and $\boldsymbol{\delta}_j$. In translational motion, $\boldsymbol{\delta}_{ij}$ can be set fixed for a specified formation, or vary smoothly for a continuously varying formation geometry. In rotational motion, it is always given as 0 to achieve consensus of rotational states.

Define

$$\begin{aligned} Q_L &= \big[\boldsymbol{q}_1^{\mathrm{T}}, \boldsymbol{q}_2^{\mathrm{T}}, \ldots, \boldsymbol{q}_N^{\mathrm{T}}\big]^{\mathrm{T}} \\ \boldsymbol{\delta}_L &= \big[\boldsymbol{\delta}_1^{\mathrm{T}}, \boldsymbol{\delta}_2^{\mathrm{T}}, \ldots, \boldsymbol{\delta}_N^{\mathrm{T}}\big]^{\mathrm{T}} \end{aligned} \tag{16}$$

and set the following assumption for the desired formation trajectory.

Assumption 3: There exists a non-negative constant $\delta_{\max}$ such that for every FWV i

$$\big\|\ddot{\boldsymbol{\delta}}_i\big\| \leq \delta_{\max} < \infty. \tag{17}$$

We have the following theorem for the estimation of the leaders.

Theorem 1: Let $\beta_1 > 0$ and $\beta_2 > \delta_{\max}$. If Assumptions 1 and 3 hold, under protocol (14), the leaders can achieve precise estimations of the desired formation states in finite time t_s, which means

$$\begin{aligned} \hat{\boldsymbol{q}}_i &= \boldsymbol{q}_0 + \boldsymbol{\delta}_{i0} \\ \hat{\boldsymbol{v}}_i &= \dot{\boldsymbol{\delta}}_i, \quad i = 1, 2, \ldots, N. \end{aligned} \tag{18}$$

Proof: Let $\tilde{\boldsymbol{v}}_i = \hat{\boldsymbol{v}}_i - \dot{\boldsymbol{\delta}}_i$ and $\tilde{\boldsymbol{q}}_i = \hat{\boldsymbol{q}}_i - \boldsymbol{q}_0 - \boldsymbol{\delta}_{i0}, i = 1, 2, \ldots, N$. Define the error vectors $\tilde{\boldsymbol{v}}_L = [\tilde{\boldsymbol{v}}_1^{\mathrm{T}}, \tilde{\boldsymbol{v}}_2^{\mathrm{T}}, \ldots, \tilde{\boldsymbol{v}}_N^{\mathrm{T}}]^{\mathrm{T}}$ and $\tilde{\boldsymbol{q}}_L = [\tilde{\boldsymbol{q}}_1^{\mathrm{T}}, \tilde{\boldsymbol{q}}_2^{\mathrm{T}}, \ldots, \tilde{\boldsymbol{q}}_N^{\mathrm{T}}]^{\mathrm{T}}$ for the velocity estimation and the position estimation, respectively. Construct the following Lyapunov function for the velocity estimation:

$$V_{\boldsymbol{v}} = \frac{1}{2} \tilde{\boldsymbol{v}}_L^{\mathrm{T}} \big[\mathcal{L}_{L1} \otimes I_p\big]^{\mathrm{T}} \tilde{\boldsymbol{v}}_L. \tag{19}$$

According to [46], taking the derivative of $V_{\boldsymbol{v}}$ yields

$$\begin{aligned} \dot{V}_{\boldsymbol{v}} &= \tilde{\boldsymbol{v}}_L^{\mathrm{T}} \big[\mathcal{L}_{L1} \otimes I_p\big]^{\mathrm{T}} \dot{\tilde{\boldsymbol{v}}}_L \\ &= \tilde{\boldsymbol{v}}_L^{\mathrm{T}} \big[\mathcal{L}_{L1} \otimes I_p\big]^{\mathrm{T}} \big[-\beta_2 \mathrm{sgn}\big(\big(\mathcal{L}_{L1} \otimes I_p\big)\tilde{\boldsymbol{v}}_L\big) - \ddot{\boldsymbol{\delta}}_L\big] \\ &\leq -\sqrt{2}(\beta_2 - \delta_{\max}) \frac{\lambda_{\min}(\mathcal{L}_{L1})}{\sqrt{\lambda_{\max}(\mathcal{L}_{L1})}} \sqrt{V_{\boldsymbol{v}}} \end{aligned} \tag{20}$$

According to Lemma 2, $\hat{\boldsymbol{v}}$ approaches its desired value $\dot{\boldsymbol{\delta}}_i$ for $i = 1, 2, \ldots, N$ in a settling time t_1

$$t_1 = \frac{\sqrt{2\lambda_{\max}(\mathcal{L}_{L1})}}{(\beta_2 - \delta_{\max})\lambda_{\min}(\mathcal{L}_{L1})}\sqrt{V_{\boldsymbol{v}}(0))}. \tag{21}$$

When $t \geq t_1$, construct a Lyapunov function $V_{\boldsymbol{q}}$

$$V_{\boldsymbol{q}} = \frac{1}{2}\tilde{\boldsymbol{q}}_L^{\mathrm{T}}\left[\mathcal{L}_{L1} \otimes I_p\right]^{\mathrm{T}}\tilde{\boldsymbol{q}}_L. \tag{22}$$

Similar as in (20)

$$\dot{V}_{\boldsymbol{q}} \leq -\sqrt{2}\beta_1 \frac{\lambda_{\min}(\mathcal{L}_{L1})}{\sqrt{\lambda_{\max}(\mathcal{L}_{L1}))}}\sqrt{V_{\boldsymbol{q}}}. \tag{23}$$

According to Lemma 2, $\hat{\boldsymbol{q}}$ approaches its desired value $\boldsymbol{q}_0 + \boldsymbol{\delta}_{i0}$ for $i = 1, 2, \ldots, N$ in a settling time t_2

$$t_2 = \frac{\sqrt{2\lambda_{\max}(\mathcal{L}_{L1})}}{\left(\beta_1 - \dot{\delta}_{\max}\right)\lambda_{\min}(\mathcal{L}_{L1})}\sqrt{V_{\boldsymbol{q}}(t_1))} + t_1. \tag{24}$$

■

Note that

$$\dot{\hat{\boldsymbol{q}}}_i - \hat{\boldsymbol{v}}_i = -\beta_1 \mathrm{sgn}\sum_{j=0}^{N} a_{ij}\left(\hat{\boldsymbol{q}}_i - \hat{\boldsymbol{q}}_j - \boldsymbol{\delta}_{ij}\right) \tag{25}$$

is bounded, and $\|\dot{\hat{\boldsymbol{q}}}_i - \hat{\boldsymbol{v}}_i\| \leq 3\beta_1$ for both the translational motion and the rotational motion.

B. Translational Motion Control

A control law for the translational motion is designed for the formation flight. The NN technique is applied to compensate for the model uncertainty. To simplify the notations, we omit the subscript i hereinafter which is the FWV index.

Consider the translational motion equation in (1) and the desired formation position in (14), the second-order dynamics can be obtained as

$$\ddot{\boldsymbol{q}}_T = M_T^{-1}(H_{IB}\boldsymbol{u}_T - G_T). \tag{26}$$

Define the tracking error as

$$\begin{aligned} \boldsymbol{e}_{T1} &= \boldsymbol{q}_T - \hat{\boldsymbol{q}}_T \\ \boldsymbol{e}_{T2} &= \dot{\boldsymbol{q}}_T - \boldsymbol{\alpha}_T \end{aligned} \tag{27}$$

where $\boldsymbol{\alpha}_T = \hat{\boldsymbol{v}}_T - A_{T1}$ and $A_{T1} = K_{T1}\boldsymbol{e}_{T1}$. $K_{T1} \in \mathbb{R}^{3\times 3}$ is a control parameter matrix for the translational motion.

Differentiating (27) with respect to time yields

$$\begin{aligned} \dot{\boldsymbol{e}}_{T1} &= \dot{\boldsymbol{q}}_T - \dot{\hat{\boldsymbol{q}}}_T \\ &= \boldsymbol{e}_{T2} - A_{T1} + \hat{\boldsymbol{v}}_T - \dot{\hat{\boldsymbol{q}}}_T \\ \dot{\boldsymbol{e}}_{T2} &= \ddot{\boldsymbol{q}}_T - \dot{\boldsymbol{\alpha}}_T \\ &= (M_T)^{-1}(H_{IB}\boldsymbol{u}_T - G_T) - \dot{\boldsymbol{\alpha}}_T. \end{aligned} \tag{28}$$

The attitude angles cannot be directly measured in this problem. We use its estimation instead. Denote $\bar{\boldsymbol{q}}_T$ the estimation of $\boldsymbol{q}_T$, and $\bar{H}_{IB}$ the estimation of H_{IB}. $\bar{H}_{IB}$ depends on $\bar{\boldsymbol{q}}_R = [\bar{\phi}, \bar{\theta}, \bar{\psi}]$, which is calculated according to the measurement of the angular velocity and the translational control information

$$\bar{H}_{IB}(\bar{\boldsymbol{q}}_R) = \begin{bmatrix} \cos\bar{\psi} & -\sin\bar{\psi} & 0 \\ \sin\bar{\psi} & \cos\bar{\psi} & 0 \\ 0 & 0 & 1 \end{bmatrix} \times \begin{bmatrix} \cos\bar{\theta} & 0 & \sin\bar{\theta} \\ 0 & 1 & 0 \\ -\sin\bar{\theta} & 0 & \cos\bar{\theta} \end{bmatrix} \times \begin{bmatrix} 1 & 0 & 0 \\ 0 & \cos\bar{\phi} & -\sin\bar{\phi} \\ 0 & \sin\bar{\phi} & \cos\bar{\phi} \end{bmatrix}. \tag{29}$$

To enhance the control performance, we use the NN technique to conpensate for model uncertainties, which is detailed in [48] and [49]. Let $z_T = [\boldsymbol{q}_T^{\mathrm{T}}, \dot{\boldsymbol{q}}_T^{\mathrm{T}}, \boldsymbol{\alpha}_T^{\mathrm{T}}, \dot{\boldsymbol{\alpha}}_T^{\mathrm{T}}, c]^{\mathrm{T}}$, where c is a constant value to fit the constant part of the uncertainty. The uncertainty part can be represented by $f_T(z_T) = G_T + M_T\dot{\boldsymbol{\alpha}}_T$. Using a constant weight matrix $W_T^* \in \mathbb{R}^{l\times 3}$, and an activation function $\boldsymbol{\xi}_T = [\xi_{T1}, \xi_{T2}, \ldots, \xi_{Tl}]^{\mathrm{T}} \in \mathbb{R}^l$, $f_i(z_T)$ can be estimated as

$$f_{iT}(z_T) = \left(W_T^*\right)^{\mathrm{T}}\boldsymbol{\xi}_T(z_T) + \epsilon \tag{30}$$

where ϵ is the estimation error with an upper bound ϵ_T, and $l > 1$ is the NN node number. The elements of activation functions are constructed using Gaussian functions

$$\xi_T^t(z_T) = \exp\left[\frac{-(z_T - \boldsymbol{\mu}_T(j))^{\mathrm{T}}\Xi_T(z_T - \boldsymbol{\mu}_T(j))}{(\eta_T(j))^2}\right] \tag{31}$$

where $j = 1, 2, \ldots, l$, η_T is the width of the Gaussian function, and μ_T is the receptive field center [50]. Different from [8] and [46], we use a diagonal weight matrix Ξ_T here to balance the order of magnitudes in vector z_T. Without Ξ_T, dimensions with higher orders of magnitudes tend to dominate the function $\xi_T^t(z_T)$, whereas dimensions with lower orders of magnitudes are usually ignored.

In (30), the weight matrix W_T^* is ideal and unknown. We use its estimation $\hat{W}_T$ instead, and update $\hat{W}_T$ according to the tracking error. The error between the estimated value and the ideal value is $\tilde{W}_T$, $\tilde{W}_T = \hat{W}_T - W_T^*$. Denote $\hat{W}_{T,k}$ the kth column vector of $\hat{W}_T$.

Since the estimation of attitude angles is used, we have to make an assumption about their boundary before we present the theorem. It can be observed that both $\bar{H}_{IB}$ and H_{IB} are bounded, therefore $H_{IB}\bar{H}_{IB}^{-1} - I$ is bounded. We introduce the unity negative-definite lemma for H_{IB}.

Lemma 3: $H_{IB}\bar{H}_{IB}^{-1} - I$ has the following properties.

1) $\boldsymbol{x}^{\mathrm{T}}(H_{IB}\bar{H}_{IB}^{-1} - I)\boldsymbol{x} \leq 0$ for all $\boldsymbol{x} \in \mathbb{R}^3$, and $\boldsymbol{x}^{\mathrm{T}}(H_{IB}\bar{H}_{IB}^{-1} - I)\boldsymbol{x} = 0$ holds only if $\bar{\boldsymbol{q}}_R = \boldsymbol{q}_R$ or $\boldsymbol{x} = \boldsymbol{0}$.
2) There exists a positive constant ϵ_h such that

$$\boldsymbol{x}^{\mathrm{T}}\left(H_{IB}\bar{H}_{IB}^{-1} - I\right)\boldsymbol{y} \leq \epsilon_h\left(\boldsymbol{x}^{\mathrm{T}}\boldsymbol{x} + \boldsymbol{y}^{\mathrm{T}}\boldsymbol{y}\right). \tag{32}$$

The proof of the lemma is in the Appendix.

Theorem 2: Given that the translational states of the desired formation trajectory are bounded in Ω_{T0}, there exist a positive constant σ_T and a parameter matrix K_{T2} such that the tracking errors for the leaders' positions [as modeled in (1) and (27)] are semiglobally uniformly ultimately bounded (SGUUB) under the control law

$$\begin{aligned} \boldsymbol{u}_T &= \bar{H}_{IB}^{-1}\left(-\boldsymbol{e}_{T1} - K_{T2}\boldsymbol{e}_{T2} + \hat{W}_T^{\mathrm{T}}\boldsymbol{\xi}_T(z_{iT})\right) \\ \dot{\hat{W}}_{T,k} &= -\left(\boldsymbol{\xi}_T(z_i)\boldsymbol{e}_{T2} + \sigma_T\hat{W}_{T,k}\right) \end{aligned} \tag{33}$$

if Assumption 2 holds. The error signals will remain within the compact sets, respectively

$$\begin{aligned}\Omega_{e_{T1}} &= \left\{\boldsymbol{e}_{T1} \in \mathbb{R}^{3\times 1} | \|\boldsymbol{e}_{T1}\| \le \sqrt{D_T}\right\}\\ \Omega_{e_{T2}} &= \left\{\boldsymbol{e}_{T2} \in \mathbb{R}^{3\times 1} | \|\boldsymbol{e}_{T2}\| \le \sqrt{D_T/\lambda_{\min}(M_T)}\right\}\\ \Omega_{\tilde{W}_T} &= \left\{\tilde{W}_T \in \mathbb{R}^{l\times 3} | \left\|\tilde{W}_T\right\| \le \sqrt{D_T}\right\}\end{aligned} \tag{34}$$

where D_T will be specified later.

Proof: Consider the following Lyapunov function:

$$V = \frac{1}{2}\boldsymbol{e}_{T1}^{\mathrm{T}}\boldsymbol{e}_{T1} + \frac{1}{2}\boldsymbol{e}_{T2}^{\mathrm{T}}M_T\boldsymbol{e}_{T2} + \frac{1}{2}\sum_{k=1}^{3}\tilde{W}_{T,k}^{\mathrm{T}}\tilde{W}_{T,k} \tag{35}$$

where $\tilde{W}_{T,k}$ is the kth column of matrix $\tilde{W}_T$. According to (28), the derivative of V is

$$\begin{aligned}\dot{V} = &-\boldsymbol{e}_{T1}^{\mathrm{T}}K_{T1}\boldsymbol{e}_{T1} + \boldsymbol{e}_{T1}^{\mathrm{T}}\left(\hat{\boldsymbol{v}}_T - \dot{\hat{\boldsymbol{q}}}_T\right)\\ &- \boldsymbol{e}_{T2}^{\mathrm{T}}[\boldsymbol{e}_{T1} + H_{IB}\boldsymbol{u}_T - G_T - M_T\dot{\boldsymbol{\alpha}}_T]\\ &- \sum_{k=1}^{3}\left[\tilde{W}_{T,k}^{\mathrm{T}}\boldsymbol{\xi}_T(z_i)\boldsymbol{e}_{T2}^{\mathrm{T}}(k) + \sigma_T\tilde{W}_{T,k}^{\mathrm{T}}\hat{W}_{T,k}\right].\end{aligned} \tag{36}$$

Substituting $\boldsymbol{u}_T$ in (33) and the NN estimation in (30) yields

$$\begin{aligned}\dot{V} \le &-\boldsymbol{e}_{T1}^{\mathrm{T}}K_{T1}\boldsymbol{e}_{T1} + \boldsymbol{e}_{T2}^{\mathrm{T}}\left[\boldsymbol{e}_{T1} + \tilde{W}_T^{\mathrm{T}}\boldsymbol{\xi}_T(z) - \hat{W}_T^{\mathrm{T}}\boldsymbol{\xi}_T(z)\right]\\ &+ \epsilon_T\|\boldsymbol{e}_{T2}\| - \boldsymbol{e}_{T2}^{\mathrm{T}}H_{IB}\bar{H}_{IB}^{-1}\left(-\boldsymbol{e}_{T1} - K_{T2}\boldsymbol{e}_{T2} + \hat{W}_T^{\mathrm{T}}\boldsymbol{\xi}_T(z_{iT})\right)\\ &+ 3\beta_1\|\boldsymbol{e}_{T1}\| - \sum_{k=1}^{3}\left[\tilde{W}_{T,k}^{\mathrm{T}}\boldsymbol{\xi}_T(z_i)\boldsymbol{e}_{T2}^{\mathrm{T}}(k) + \sigma_T\tilde{W}_{T,k}^{\mathrm{T}}\hat{W}_{T,k}\right]\\ \le &-\boldsymbol{e}_{T1}^{\mathrm{T}}K_{T1}\boldsymbol{e}_{T1} - \boldsymbol{e}_{T2}^{\mathrm{T}}K_{T2}\boldsymbol{e}_{T2} + \epsilon_T\|\boldsymbol{e}_{T2}\| + 3\beta_1\|\boldsymbol{e}_{T1}\|\\ &- \boldsymbol{e}_{T2}^{\mathrm{T}}\left(H_{IB}\bar{H}_{IB}^{-1} - I\right)\left(-\boldsymbol{e}_{T1} - K_{T2}\boldsymbol{e}_{T2} + \hat{W}_T^{\mathrm{T}}\boldsymbol{\xi}_T(z_{iT})\right)\\ &- \sum_{k=1}^{3}\sigma_T\tilde{W}_{T,k}^{\mathrm{T}}\hat{W}_{T,k}\end{aligned} \tag{37}$$

in which

$$\begin{aligned}&-\sigma_T\tilde{W}_{T,k}^{\mathrm{T}}\hat{W}_{T,k}\\ &= -\sigma_T\tilde{W}_{T,k}^{\mathrm{T}}\left(\tilde{W}_{T,k} + W_T^*(k)\right)\\ &\le -\sigma_T\left\|\tilde{W}_{T,k}\right\|^2 + \frac{\sigma_T}{2}\left\|\tilde{W}_{T,k}\right\|^2 + \frac{\sigma_T}{2}\left\|W_T^*(k)\right\|^2\\ &\le \frac{\sigma_T}{2}\left(\left\|W_{T,k}^*\right\|^2 - \left\|\tilde{W}_{T,k}\right\|^2\right).\end{aligned} \tag{38}$$

According to Lemma 3

$$\begin{aligned}\dot{V} \le &-\boldsymbol{e}_{T1}^{\mathrm{T}}K_{T1}\boldsymbol{e}_{T1} - \boldsymbol{e}_{T2}^{\mathrm{T}}K_{T2}\boldsymbol{e}_{T2} + 3\beta_1\|\boldsymbol{e}_{T1}\|\\ &+ \epsilon_h\left(3\boldsymbol{e}_{T2}^{\mathrm{T}}\boldsymbol{e}_{T2} + \boldsymbol{e}_{T1}^{\mathrm{T}}\boldsymbol{e}_{T1} + \left\|\tilde{W}_T^{\mathrm{T}}\boldsymbol{\xi}_T(z_{iT}))\right\|^2\right)\\ &+ \sum_{k=1}^{3}\frac{\sigma_T}{2}\left(\left\|W_{T,k}^*\right\|^2 - \left\|\tilde{W}_{T,k}\right\|^2\right) + \epsilon_T\|\boldsymbol{e}_{T2}\|\\ &+ \epsilon_h\left\|\left(W_T^*\right)^{\mathrm{T}}\boldsymbol{\xi}_T(z_{iT})\right\|^2.\end{aligned} \tag{39}$$

Since $\boldsymbol{\xi}_T(z_{iT})$ is a Gaussian function and stays in the range $(0, 1)$, for both W_T^* and $\tilde{W}_T^{\mathrm{T}}$

$$\begin{aligned}\left\|W_T^{\mathrm{T}}\boldsymbol{\xi}_T(z_{iT})\right\|^2 &\le \sum_{m=1}^{3}\sum_{n=1}^{3}\sum_{k=1}^{3}W_T(m,k)W_T(n,k)\\ &\le \sum_{m=1}^{3}\sum_{n=1}^{3}\sum_{k=1}^{3}\frac{W_T^2(m,k) + W_T^2(n,k)}{2}\\ &\le \sum_{n=1}^{3}\sum_{k=1}^{3}3W_T^2(n,k)\\ &\le 3\sum_{k=1}^{3}\left\|W_{T,k}\right\|^2\end{aligned} \tag{40}$$

where $W_T(m,k)$ is the element in the mth row and the kth column of matrix W_T.

Then, the derivative of the Lyapunov function becomes

$$\begin{aligned}\dot{V} \le &-\boldsymbol{e}_{T1}^{\mathrm{T}}(K_{T1} - \epsilon_h)\boldsymbol{e}_{T1} - \boldsymbol{e}_{T2}^{\mathrm{T}}(K_{T2} - 3\epsilon_h)\boldsymbol{e}_{T2}\\ &+ \epsilon_T\|\boldsymbol{e}_{T2}\| + 3\beta_1\|\boldsymbol{e}_{T1}\|\\ &+ \sum_{k=1}^{3}\frac{\sigma_T + 6\epsilon_h}{2}\left\|W_T^*(k)\right\|^2 - \sum_{k=1}^{3}\frac{\sigma_T - 6\epsilon_h}{2}\left\|\tilde{W}_{T,k}\right\|^2\\ \le &-\rho_T V + \varrho_T\sqrt{V} + c_T\end{aligned} \tag{41}$$

where ρ_T, ϱ_T, and c_T are the three constants

$$\begin{aligned}\rho_T &= \min\Big(2\lambda_{\min}(K_{T1} - \epsilon_h), 2\lambda_{\min}(K_{T2} - 3\epsilon_h)M_T^{-1}\\ &\qquad \sigma_T - 6\epsilon_h)\\ \varrho_T &= \max\left(3\sqrt{2}\beta_1, \epsilon_T\sqrt{2M_T^{-1}}\right)\\ c_T &= \sum_{k=1}^{3}\frac{\sigma_T + 6\epsilon_h}{2}\left\|W_{T,k}^*\right\|^2.\end{aligned} \tag{42}$$

Note that

$$\dot{V} \le \begin{cases}-(\rho_T - \varrho_T)V + c_T, & \text{if } V > 1\\ -\rho_T V + (\varrho_T + c_T), & \text{if } V \le 1.\end{cases} \tag{43}$$

$\dot{V}$ can be further represented as

$$\dot{V} \le -\rho_T' V + c_T' \tag{44}$$

where

$$\begin{aligned}\rho_T' &= \rho_T - \varrho_T\\ c_T' &= c_T + \varrho_T.\end{aligned} \tag{45}$$

Design control gain matrices K_{T1}, K_{T2}, and σ_T such that

$$\begin{aligned}\lambda_{\min}(K_{T1}) &> \epsilon_h + 0.5\varrho_T\\ \lambda_{\min}(K_{T2}) &> 3\epsilon_h + 0.5\varrho_T\lambda_{\max}(M_T)\\ \sigma_T &> 6\epsilon_h + \varrho_T.\end{aligned} \tag{46}$$

$\rho_T' > 0$ can be assured. Then, we have

$$\begin{aligned}V(t) &\le V(0)\exp\left(-\rho_T' t\right) + \frac{c_T'}{\rho_T'}\left(1 - \exp\left(-\rho_T' t\right)\right)\\ &\le V(0) + \frac{c_T'}{\rho_T'} = 2D_T\end{aligned} \tag{47}$$

therefore the tracking errors $\boldsymbol{e}_{T1}$, $\boldsymbol{e}_{T2}$, and $\tilde{W}_T$ are SGUUB as in (34). ■

C. Attitude Estimation

For FWVs, gyroscopes are used to measure angular velocities, whereas attitude angles cannot be measured directly by onboard sensors. They are always achieved by integrating the angular velocities, and the integration process leads to error

accumulation. To address this problem, we design an estimation algorithm for attitude angles and analyze the stability of the algorithm.

Based on the observation that the rotational states and the translational states are coupled by coordinate transform, we estimate attitude angles according to the variation of the translational states.

Substituting (33) into (28) yields

$$\begin{aligned} & M_T\dot{\boldsymbol{e}}_{T2} + M_T\dot{\boldsymbol{\alpha}}_T + G_T \\ &= M_T\dot{\boldsymbol{e}}_{T,2} + \left(W_T^*\right)^{\mathrm{T}}\boldsymbol{\xi}_T + \epsilon \\ &= H_{IB}\bar{H}_{IB}^{-1}\Big[-\boldsymbol{e}_{T1} - K_{T2}\boldsymbol{e}_{T2} + \hat{W}_T^{\mathrm{T}}\boldsymbol{\xi}_T\Big]. \end{aligned} \tag{48}$$

Let $\boldsymbol{\gamma}_1 = M_T\dot{\boldsymbol{e}}_{T2} + \hat{W}_T^{\mathrm{T}}\boldsymbol{\xi}_T$, $\boldsymbol{\gamma}_2 = -\boldsymbol{e}_{T1} - K_{T2}\boldsymbol{e}_{T2} + \hat{W}_T^{\mathrm{T}}\boldsymbol{\xi}_T$, and $\eta = \epsilon - \tilde{W}_T^{\mathrm{T}}\boldsymbol{\xi}_T$, we have

$$\boldsymbol{\gamma}_1 + \eta = H_{IB}\bar{H}_{IB}^{-1}\boldsymbol{\gamma}_2. \tag{49}$$

Denote $\tilde{\boldsymbol{q}}_R = \boldsymbol{q}_R - \bar{\boldsymbol{q}}_R$ as the difference between $\boldsymbol{q}_R$ and its estimated value. The second-order approximation to an arbitrary function $f(\boldsymbol{q}_R)$ around $\tilde{\boldsymbol{q}}_R$ is

$$\begin{aligned} f(\boldsymbol{q}_R) = {} & f(\bar{\boldsymbol{q}}_R) + \tilde{\boldsymbol{q}}_R^{\mathrm{T}}\nabla f(\boldsymbol{q}_R) + 0.5\tilde{\boldsymbol{q}}_R^{\mathrm{T}}\mathcal{H}(f)\tilde{\boldsymbol{q}}_R \\ & + O\big(f(\boldsymbol{q}_R)\big) \end{aligned} \tag{50}$$

where $\nabla f(\boldsymbol{q}_R)$ is the gradient matrix, $\mathcal{H}(f)$ is the Hessian matrix at $\bar{\boldsymbol{q}}_R$, and $O(f(\boldsymbol{q}_R))$ contains the higher order terms.

Approximate each element in H_{IB} based on $\bar{H}_{IB}$ as in (50), and substitute the approximation to (48)

$$\begin{aligned} & \boldsymbol{\gamma}_1 - \boldsymbol{\gamma}_2 + O\big(H_{IB}(\boldsymbol{q}_R)\big) + \eta \\ &= \sum_m \tilde{\boldsymbol{q}}_R(m)\nabla_{\boldsymbol{q}_R(m)}\bar{H}_{IB}(\boldsymbol{q}_R)\boldsymbol{\gamma}_2 \\ &\quad + \frac{1}{2}\sum_m\sum_n \tilde{\boldsymbol{q}}_R(m)\tilde{\boldsymbol{q}}_R(n)\mathcal{H}_{m,n}(\boldsymbol{q}_R)\boldsymbol{\gamma}_2. \end{aligned} \tag{51}$$

In the above equation

$$\begin{aligned} \nabla_{\boldsymbol{q}_R(m)}\bar{H}_{IB}(\boldsymbol{q}_R) &= \frac{\partial \bar{H}_{IB}(\boldsymbol{q}_R)}{\partial \boldsymbol{q}_R(m)} \\ \mathcal{H}_{m,n}(\boldsymbol{q}_R) &= \frac{\partial^2 \bar{H}_{IB}(\boldsymbol{q}_R)}{\partial \boldsymbol{q}_R(m)\partial \boldsymbol{q}_R(n)} = \frac{\partial^2 \bar{H}_{IB}(\boldsymbol{q}_R)}{\partial \boldsymbol{q}_R(n)\partial \boldsymbol{q}_R(m)}. \end{aligned} \tag{52}$$

Property 2: $\nabla_{\boldsymbol{q}_R(m)}\bar{H}_{IB}(\boldsymbol{q}_R)$, $\mathcal{H}_{m,n}(\boldsymbol{q}_R)$, and $O(H_{IB})$ are all bounded.

Remark 8: According to (29), all the elements in $\bar{H}_{IB}(\boldsymbol{q}_R)$ are the sums of products of sine and cosine functions. Any order of the partial differential term of $\bar{H}_{IB}(\boldsymbol{q}_R)$ is also a combination of sine and cosine functions. Therefore, we can easily obtain Property 2.

Ignore the high-order terms $O(H_{IB}(\boldsymbol{q}_R))$ and the small value η, we can approximate the estimation error $\tilde{\boldsymbol{q}}_R$ by solving the following equation:

$$\begin{aligned} \boldsymbol{\gamma}_1 - \boldsymbol{\gamma}_2 = {} & \sum_m \bar{\tilde{\boldsymbol{q}}}_R(m)\nabla_{\boldsymbol{q}_R(m)}\bar{H}_{IB}(\boldsymbol{q}_R)\boldsymbol{\gamma}_2 \\ & + \frac{1}{2}\sum_m\sum_n \bar{\tilde{\boldsymbol{q}}}_R(m)\bar{\tilde{\boldsymbol{q}}}_R(n)\mathcal{H}_{m,n}(\boldsymbol{q}_R)\boldsymbol{\gamma}_2. \end{aligned} \tag{53}$$

Denote $\bar{\tilde{\boldsymbol{q}}}_R$ the solution of (53), and $\tilde{\tilde{\boldsymbol{q}}}_R = \tilde{\boldsymbol{q}}_R - \bar{\tilde{\boldsymbol{q}}}_R$ the difference between the estimation error and its calculated solution. The following lemma can be achieved.

Lemma 4: There exists a positive constant $\epsilon_{\boldsymbol{q}}$ such that

$$\left\|\tilde{\tilde{\boldsymbol{q}}}_R\right\| \le \epsilon_{\boldsymbol{q}}. \tag{54}$$

Proof: Substituting $\tilde{\boldsymbol{q}}_R = \tilde{\tilde{\boldsymbol{q}}}_R + \bar{\tilde{\boldsymbol{q}}}_R$ into (53) yields

$$\begin{aligned} & \boldsymbol{\gamma}_1 - \boldsymbol{\gamma}_2 + O\big(H_{IB}(\boldsymbol{q}_R)\big) + \eta \\ &= \sum_m \bar{\tilde{\boldsymbol{q}}}_R(m)\nabla_{\boldsymbol{q}_R(m)}\bar{H}_{IB}(\boldsymbol{q}_R)\boldsymbol{\gamma}_2 \\ &\quad + \frac{1}{2}\sum_m\sum_n \bar{\tilde{\boldsymbol{q}}}_R(m)\bar{\tilde{\boldsymbol{q}}}_R(n)\mathcal{H}_{m,n}(\boldsymbol{q}_R)\boldsymbol{\gamma}_2 \\ &\quad + \sum_m \tilde{\tilde{\boldsymbol{q}}}_R(m)\nabla_{\boldsymbol{q}_R(m)}\bar{H}_{IB}(\boldsymbol{q}_R)\boldsymbol{\gamma}_2 \\ &\quad + \sum_m\sum_n \left(\frac{1}{2}\tilde{\tilde{\boldsymbol{q}}}_R^2(m) + \tilde{\tilde{\boldsymbol{q}}}_R(m)\bar{\tilde{\boldsymbol{q}}}_R(n)\right)\mathcal{H}_{m,n}(\boldsymbol{q}_R)\boldsymbol{\gamma}_2 \\ &= \boldsymbol{\gamma}_1 - \boldsymbol{\gamma}_2 + \sum_m \tilde{\tilde{\boldsymbol{q}}}_R(m)\nabla_{\boldsymbol{q}_R(m)}\bar{H}_{IB}(\boldsymbol{q}_R)\boldsymbol{\gamma}_2 \\ &\quad + \sum_m\sum_n \left(\frac{1}{2}\tilde{\tilde{\boldsymbol{q}}}_R^2(m) + \tilde{\tilde{\boldsymbol{q}}}_R(m)\bar{\tilde{\boldsymbol{q}}}_R(n)\right)\mathcal{H}_{m,n}(\boldsymbol{q}_R)\boldsymbol{\gamma}_2. \end{aligned} \tag{55}$$

Therefore

$$\begin{aligned} O(H_{IB}) + \eta = {} & \sum_m \tilde{\tilde{\boldsymbol{q}}}_R(m) \\ & \times \left[\nabla_{\boldsymbol{q}_R(m)}\bar{H}_{IB} + \sum_n \left(\frac{1}{2}\tilde{\tilde{\boldsymbol{q}}}_R(m) + \bar{\tilde{\boldsymbol{q}}}_R(n)\right)\mathcal{H}_{m,n}\right]\boldsymbol{\gamma}_2 \end{aligned} \tag{56}$$

where η and $\boldsymbol{\gamma}_2$ are bounded according to Theorem 2, $\nabla_{\boldsymbol{q}_R(m)}H_{IB}$, $\mathcal{H}_{m,n}$, and $O(H_{IB})$ are bounded according to Property 2.

Suppose that there does not exist a positive constant $\epsilon_{\boldsymbol{q}}$ which satisfies (54), there will be a dimension m such that $\tilde{\tilde{\boldsymbol{q}}}_R(m)$ goes to infinity, which contradicts the bounding property of $O(H_{IB}) + \eta$ in (56). Therefore, Lemma 4 holds. ■

Remark 9: In simulations, we choose only the feasible solution of (53) as the calculated estimation error. Feasible here means that the solution satisfies the physical constraints of attitude angles.

Theorem 3: Under Property 2 and Lemma 4, the estimation error of attitude angles is SGUUB under the estimation law

$$\dot{\bar{\boldsymbol{q}}}_R = \bar{\boldsymbol{\nu}}_R + \sigma_{\boldsymbol{\nu}}\bar{\tilde{\boldsymbol{q}}}_R \tag{57}$$

if Assumption 2 holds. The estimation error will remain within the compact set

$$\Omega_{\tilde{\boldsymbol{q}}_R} = \left\{\tilde{\boldsymbol{q}}_R \in \mathbb{R}^{3\times 1} \,|\, \left\|\tilde{\boldsymbol{q}}_R\right\| \le \epsilon_{\boldsymbol{\nu}}/\sigma_{\boldsymbol{\nu}} + \epsilon_{\boldsymbol{q}}\right\}. \tag{58}$$

Proof: Construct a Lyapunov function with respect to the estimation error $\tilde{\boldsymbol{q}}_R$

$$V = \frac{1}{2}\tilde{\boldsymbol{q}}_R^{\mathrm{T}}\tilde{\boldsymbol{q}}_R. \tag{59}$$

Substituting (57) into the derivative of V yields

$$\begin{aligned} \dot{V} &= \tilde{\boldsymbol{q}}_R^{\mathrm{T}}(\dot{\boldsymbol{q}}_R - \dot{\bar{\boldsymbol{q}}}_R) \\ &= \tilde{\boldsymbol{q}}_R^{\mathrm{T}}\left(\boldsymbol{\nu}_R - \bar{\boldsymbol{\nu}}_R - \sigma_{\boldsymbol{\nu}}\bar{\tilde{\boldsymbol{q}}}_R\right) \end{aligned}$$

$$= \tilde{\boldsymbol{q}}_R^{\mathrm{T}}\Big[\tilde{\boldsymbol{v}}_R - \sigma_v\Big(\tilde{\boldsymbol{q}}_R - \tilde{\tilde{\boldsymbol{q}}}_R\Big)\Big]$$
$$\leq -\sigma_v \tilde{\boldsymbol{q}}_R^{\mathrm{T}}\tilde{\boldsymbol{q}}_R + \big\|\tilde{\boldsymbol{q}}_R\big\|\Big(\|\tilde{\boldsymbol{v}}_R\| + \sigma_v\Big\|\tilde{\tilde{\boldsymbol{q}}}_R\Big\|\Big). \tag{60}$$

Applying Lemma 4 and Assumption 2

$$\dot{V} \leq -\big(\sigma_v\big\|\tilde{\boldsymbol{q}}_R\big\| - \big(\epsilon_v + \sigma_v\epsilon_q\big)\big)\sqrt{2V}$$
$$\leq -f\big(\boldsymbol{q}_R\big)\sqrt{2V}. \tag{61}$$

If $\|\tilde{\boldsymbol{q}}_R\| > \epsilon_v/\sigma_v + \epsilon_v$, $f(\boldsymbol{q}_R) > 0$ and $\dot{V} < 0$, the estimation error $\|\tilde{\boldsymbol{q}}_R\|$ keeps decreasing until it goes into the region as in (58). Hence, it is straight forward to present that the estimation error $\|\tilde{\boldsymbol{q}}_R\|$ is SGUUB and will finally remain in the region $\Omega_{\tilde{\boldsymbol{q}}_R}$, which completes the proof. ■

Remark 10: According to (58) and Theorem 3, the estimation error of the attitude angle is very related to the measuring accuracy of the angular velocity $\tilde{\boldsymbol{v}}_R$ and the calculation error $\tilde{\tilde{\boldsymbol{q}}}_R$. We can achieve the estimation of attitude angles with higher accuracy by improving the measuring accuracy of $\bar{\boldsymbol{v}}_R$ and calculating accuracy of $\tilde{\boldsymbol{q}}_R$.

D. Rotational Motion Control

Given the desired formation attitude angles and angular velocities as in (14), the rotational control algorithm can be designed. Consider the rotational motion equation in (6), the second-order dynamics can be obtained as

$$\ddot{\boldsymbol{q}}_R = M_{iR}^{-1}\big(\boldsymbol{u}_R - C_R\dot{\boldsymbol{q}}_R\big). \tag{62}$$

Although attitude angles are achieved by estimation and angular velocities are measured inaccurately, the stability of the system is analyzed using real states

$$\boldsymbol{e}_{R1} = \boldsymbol{q}_R - \hat{\boldsymbol{q}}_R$$
$$\boldsymbol{e}_{R2} = \boldsymbol{v}_R - \boldsymbol{\alpha}_R. \tag{63}$$

Estimated error signals are also calculated

$$\bar{\boldsymbol{e}}_{R1} = \bar{\boldsymbol{q}}_R - \hat{\boldsymbol{q}}_R = \boldsymbol{e}_{R1} + \bar{\boldsymbol{q}}_R - \boldsymbol{q}_R$$
$$\bar{\boldsymbol{e}}_{R2} = \bar{\boldsymbol{v}}_R - \bar{\boldsymbol{\alpha}}_R = \boldsymbol{e}_{R2} - \tilde{\boldsymbol{v}}_R + K_{R2}\big(\boldsymbol{q}_R - \bar{\boldsymbol{q}}_R\big) \tag{64}$$

where $\boldsymbol{\alpha}_R = \hat{\boldsymbol{v}}_R - A_{R1}$, $A_{R1} = K_{R1}\boldsymbol{e}_{R1}$, $\bar{\boldsymbol{\alpha}}_R = \hat{\boldsymbol{v}}_R - \bar{A}_{R1}$, and $\bar{A}_{R1} = K_{R1}\bar{\boldsymbol{e}}_{R1}$.

Substituting $\dot{\boldsymbol{q}}_R = \boldsymbol{v}_R$ and differentiating (63) with respect to time yields

$$\dot{\boldsymbol{e}}_{R1} = \dot{\boldsymbol{q}}_R - \dot{\hat{\boldsymbol{q}}}_R = \boldsymbol{e}_{R2} - A_{R1} + \hat{\boldsymbol{v}}_R - \dot{\hat{\boldsymbol{q}}}_R$$
$$\dot{\boldsymbol{e}}_{R2} = \dot{\boldsymbol{q}}_R - \dot{\boldsymbol{\alpha}}_R = M_R^{-1}\big(\boldsymbol{u}_R - C_R\dot{\boldsymbol{q}}_R\big) - \dot{\boldsymbol{\alpha}}_R. \tag{65}$$

The NN technique is also used in the rotational motion to compensate for model uncertainties, estimation error, and measurement inaccuracy. Let $\boldsymbol{z}_R = [\bar{\boldsymbol{q}}_R^{\mathrm{T}}, \boldsymbol{v}_R^{\mathrm{T}}, \boldsymbol{\alpha}_R^{\mathrm{T}}, \dot{\boldsymbol{\alpha}}_R^{\mathrm{T}}]^{\mathrm{T}}$, the NN function is constructed as

$$f_R(\boldsymbol{z}_R) = C_R\dot{\boldsymbol{q}}_R + M_R\dot{\boldsymbol{\alpha}}_R$$
$$- \Big(1 + K_{R2}^2\Big)\big(\boldsymbol{q}_R - \bar{\boldsymbol{q}}_R\big) - K_{R2}\tilde{\boldsymbol{v}}_R. \tag{66}$$

Equation (66) can also be described using a constant weight matrix $W_R^* \in \mathbb{R}^{l\times 3}$ and an activation function $\boldsymbol{\xi}_R = [\xi_{R1}, \xi_{R2}, \ldots, \xi_{Rl}]^{\mathrm{T}} \in \mathbb{R}^l$

$$f_R(\boldsymbol{z}_T) = \big(W_R^*\big)^{\mathrm{T}}\boldsymbol{\xi}_R(\boldsymbol{z}_R) + \epsilon \tag{67}$$

where ϵ has an upper bound ϵ_R. The weight matrix W_R^* is ideal and unknown. We use its estimation $\hat{W}_R$ instead, and update $\hat{W}_R$ according to the tracking error. The error between the estimated value and the ideal value is $\tilde{W}_R$, $\tilde{W}_R = \hat{W}_R - W_R^*$. Denote $\boldsymbol{e}_{R2}(k)$ and $\hat{W}_{R,k}$ the kth element and the kth column vector of $\boldsymbol{e}_{R2}$ and $\hat{W}_R$, respectively.

Theorem 4: Given that the rotational states of the desired trajectory are bounded in Ω_{R0}, the tracking errors for the leaders' angles [as modeled in (6) and (63)] are SGUUB under the control law

$$\boldsymbol{u}_R = -\Big(\bar{\boldsymbol{e}}_{R1} + K_{R2}\bar{\boldsymbol{e}}_{R2} - \hat{W}_R^{\mathrm{T}}\boldsymbol{\xi}_R(\boldsymbol{z}_R)\Big)$$
$$\dot{\hat{W}}_{R,k} = -\Big(\boldsymbol{\xi}_R(z)\boldsymbol{e}_{R2}(k) + \sigma_R\hat{W}_{R,k}\Big). \tag{68}$$

The error signals will remain within the compact sets, respectively

$$\Omega_{e_{R1}} = \Big\{\boldsymbol{e}_{R1} \in \mathbb{R}^{3\times 1} \big| \|\boldsymbol{e}_{R1}\| \leq \sqrt{D_R}\Big\}$$
$$\Omega_{e_{R2}} = \Big\{\boldsymbol{e}_{R2} \in \mathbb{R}^{3\times 1} \big| \|\boldsymbol{e}_{R2}\| \leq \sqrt{D_R/\gamma_{\min}(M_R)}\Big\}$$
$$\Omega_{\tilde{W}_R} = \Big\{\tilde{W}_R \in \mathbb{R}^{l\times 3} \big| \big\|\tilde{W}_R\big\| \leq \sqrt{D_R}\Big\} \tag{69}$$

where D_R will be detailed later.

Proof: Consider the following Lyapunov function:

$$V = \frac{1}{2}\boldsymbol{e}_{R1}^{\mathrm{T}}\boldsymbol{e}_{R1} + \frac{1}{2}\boldsymbol{e}_{R2}^{\mathrm{T}}M_R\boldsymbol{e}_{R2} + \frac{1}{2}\sum_{k=1}^{3}\tilde{W}_R^{\mathrm{T}}\tilde{W}_R. \tag{70}$$

According to (63), (64), and (68), the derivative of V is

$$\dot{V} = \boldsymbol{e}_{R1}^{\mathrm{T}}\Big(\boldsymbol{e}_{R2} - K_{R1}\boldsymbol{e}_{R1} + \hat{\boldsymbol{v}}_R - \dot{\hat{\boldsymbol{q}}}_R\Big)$$
$$+ \boldsymbol{e}_{R2}^{\mathrm{T}}\Big[-\bar{\boldsymbol{e}}_{R1} - K_{R2}\bar{\boldsymbol{e}}_{R2} + \hat{W}_R^{\mathrm{T}}\boldsymbol{\xi}_R(z_R) - C_R\dot{\boldsymbol{q}}_R - M_R\dot{\boldsymbol{\alpha}}_R\Big]$$
$$- \sum_{k=1}^{3}\Big[\tilde{W}_{R,k}^{\mathrm{T}}\boldsymbol{\xi}_R(z)\boldsymbol{e}_{R2}(k) + \sigma_R\tilde{W}_{R,k}^{\mathrm{T}}\hat{W}_{R,k}\Big]$$
$$\leq -\boldsymbol{e}_{R1}^{\mathrm{T}}K_{R1}\boldsymbol{e}_{R1} - \boldsymbol{e}_{R2}^{\mathrm{T}}K_{R2}\boldsymbol{e}_{R2} + 3\beta_1\|\boldsymbol{e}_{R1}\|$$
$$+ \boldsymbol{e}_{R2}^{\mathrm{T}}\Big[\Big(1 + K_{R2}^2\Big)\big(\boldsymbol{q}_R - \bar{\boldsymbol{q}}_R\big) + K_{R2}\tilde{\boldsymbol{v}}_R\Big]$$
$$+ \boldsymbol{e}_{R2}^{\mathrm{T}}\Big[\hat{W}_R^{\mathrm{T}}\boldsymbol{\xi}_R(z_R) - C_R\dot{\boldsymbol{q}}_R - M_R\dot{\boldsymbol{\alpha}}_R\Big]$$
$$- \sum_{k=1}^{3}\Big[\tilde{W}_{R,k}^{\mathrm{T}}\boldsymbol{\xi}_R(z)\boldsymbol{e}_{R2}(k) + \sigma_R\tilde{W}_{R,k}^{\mathrm{T}}\hat{W}_{R,k}\Big]. \tag{71}$$

Substituting (66) and (33) into (71) yields

$$\dot{V} \leq -\boldsymbol{e}_{R1}^{\mathrm{T}}K_{R1}\boldsymbol{e}_{R1} - \boldsymbol{e}_{R2}^{\mathrm{T}}K_{R2}\boldsymbol{e}_{R2} + 3\beta_1\|\boldsymbol{e}_{R1}\| + \epsilon_R\|\boldsymbol{e}_{R2}\|$$
$$- \sum_{k=1}^{3}\sigma_R\tilde{W}_{R,k}^{\mathrm{T}}\hat{W}_{R,k} \tag{72}$$

where

$$-\tilde{W}_{R,k}^{\mathrm{T}}\hat{W}_{T,k} \leq \frac{1}{2}\Big(\big\|W_R^*(k)\big\|^2 - \big\|\tilde{W}_{R,k}\big\|^2\Big). \tag{73}$$

Therefore

$$\dot{V} = -\boldsymbol{e}_{R1}^{\mathrm{T}}K_{R1}\boldsymbol{e}_{R1} - \boldsymbol{e}_{R2}^{\mathrm{T}}K_{R2}\boldsymbol{e}_{R2} - \frac{\sigma_R}{2}\sum_{k=1}^{3}\big\|\tilde{W}_{R,k}^{\mathrm{T}}\big\|^2$$
$$+ 3\beta_1\|\boldsymbol{e}_{R1}\| + \epsilon_R\|\boldsymbol{e}_{R2}\| + \frac{\sigma_R}{2}\sum_{k=1}^{3}\|W_R^*(k)\|^2$$

$$\leq -\rho_R V + \varrho_R \sqrt{V} + c_R \tag{74}$$

where ρ_{iR} and c_{iR} are two constants

$$\rho_R = \min(2\lambda_{\min}(K_{R1}), 2\lambda_{\min}(K_{R2}), \sigma_R) \tag{75}$$
$$\varrho_R = \max\left(\sqrt{2M_R^{-1}}\epsilon_R, 3\sqrt{2}\beta_1\right)$$

$$c_R = \sum_{k=1}^{3} \frac{\sigma_R}{2} \left\| W_R^*(k) \right\|^2. \tag{76}$$

Note that

$$\dot{V} \leq \begin{cases} -(\rho_R - \varrho_R)V + c_R, & \text{if } V > 1 \\ -\rho_R V + (\varrho_R + c_R), & \text{if } V \leq 1 \end{cases}. \tag{77}$$

$\dot{V}$ can be further represented as

$$\dot{V} \leq -\rho_R' V + c_R' \tag{78}$$

where

$$\rho_R' = \rho_R - \varrho_R$$
$$c_R' = c_R + \varrho_R. \tag{79}$$

Design control gain matrices K_{R1}, K_{R2}, and σ_R such that $\lambda_{\min}(K_{R1}) > 0.5\varrho_R$, $\lambda_{\min}(K_{R2}) > 0.5\varrho_R$, and $\sigma_T > \varrho_R$, $\rho_T' > 0$ is always assured. Then

$$V(t) \leq V(0)\exp\left(-\rho_R' t\right) + \frac{c_R'}{\rho_R'}\left(1 - \exp\left(-\rho_R' t\right)\right)$$
$$\leq V(0) + \frac{c_R'}{\rho_R'} = 2D_R. \tag{80}$$

Therefore, the tracking errors $\boldsymbol{e}_{R1}$, $\boldsymbol{e}_{R2}$, and $\tilde{W}_R$ are SGUUB and remain within the compact sets as in (69). ■

E. Formation Control for the Followers

Assume that the leaders and the followers are isomorphic, the follower model is also presented in (1), (6), and (7). The control objective of this part is to keep the followers in a convex hull with respect to the leaders. The followers should move with the leaders.

The following estimation algorithm is used to estimate the desired translational and rotational information of the followers:

$$\dot{\hat{\boldsymbol{q}}}_i = \hat{\boldsymbol{v}}_i - \beta_3 \text{sgn} \sum_{j=N+1}^{N+M} a_{ij}(\hat{\boldsymbol{q}}_i - \hat{\boldsymbol{q}}_j)$$
$$\dot{\hat{\boldsymbol{v}}}_i = -\beta_4 \text{sgn} \sum_{j=N+1}^{N+M} a_{ij}(\hat{\boldsymbol{v}}_i - \hat{\boldsymbol{v}}_j). \tag{81}$$

The definition of $\hat{\boldsymbol{q}}_i$ and $\hat{\boldsymbol{v}}_i$ is similar as in Section III-A. Note that $i = N+1, N+2, \ldots, N+M$ for the followers. The precise estimation of the desired follower states can be achieved in the limited time.

The translational motion and the rotational control problem for the followers can also be handled separately as in Sections III-B–III-D.

TABLE I
PARAMETERS FOR SIMULATION

Parameters	Values	Parameters	Values
K_{T1}	I_3	K_{R1}	I_3
K_{T2}	$8I_3$	K_{R2}	$8I_3$
β_1	5	σ_T	4
β_2	2.5	σ_R	4
β_3	5	σ	0.5
β_4	2.5		

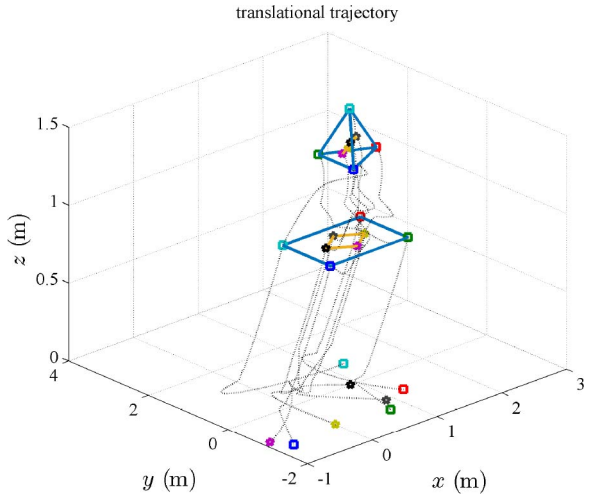

Fig. 2. Translational trajectories of eight FWVs with a time-varying formation.

IV. SIMULATION

Simulation is conducted to demonstrate the effectiveness of the proposed algorithm. The FWV model is formulated in Section II-B, where $m_i = 0.0056$ kg

$$\bar{I}_p = \begin{bmatrix} 5.75 \times 10^{-7} & 0 & 0 \\ 0 & 5.76 \times 10^{-7} & 0 \\ 0 & 0 & 9.97 \times 10^{-7} \end{bmatrix} \text{kg} \cdot \text{m}^2.$$

A group of eight FWVs is considered for the formation problem, four of them are leaders labeled as 1, 2, 3, and 4, and the other four are followers labeled as 5, 6, 7, and 8. The trajectory of the formation is preset manually. The simulation parameters are presented in Table I.

The initial positions of the FWVs are randomly set. The relative motion of the formation is desired to switch at 50 s. In the first 50 s, the leaders and the followers are required to form a square, respectively. In the last 50 s, the shape of the leaders is required to change to a triangular pyramid, whereas the shape of followers is still required to be a square that rotates in the space.

Fig. 2 illustrates the 3-D trajectories of the FWVs. Figs. 3 and 4 show the translational tracking errors of the leaders and the followers, respectively. Figs. 5 and 6 plot the rotational tracking errors of the FWVs. Other simulation results are not presented here due to the page limitation. It can be observed that all the FWV states converge within 10 s.

As discussed in Remark 6, the desired distance $\boldsymbol{\delta}_{ij}$ can be designed fixed for a constant formation configuration, or smoothly varying for a time-varying configuration. Actually,

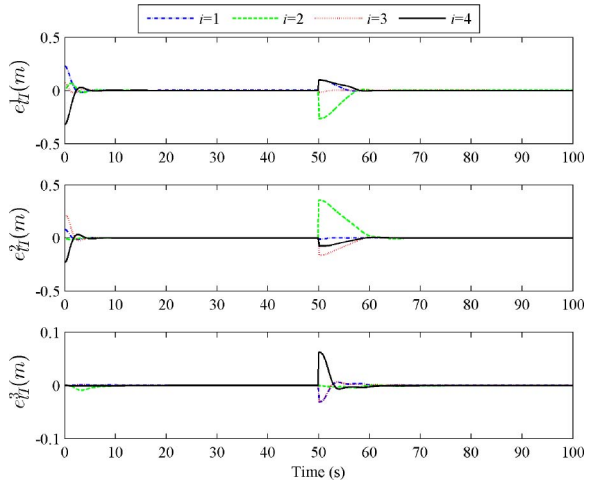

Fig. 3. Translational errors of the leaders with switched δ_{iT}.

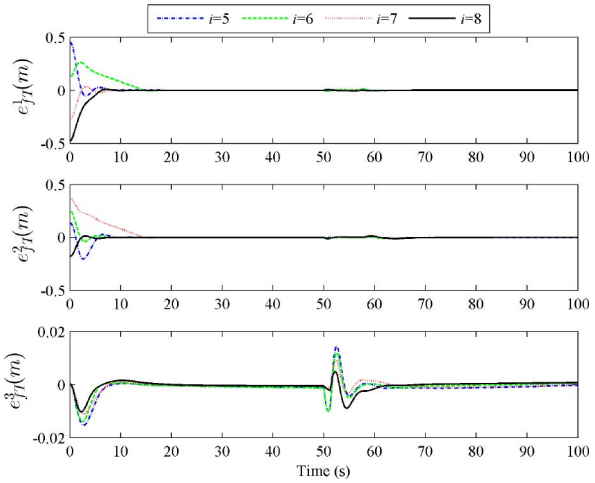

Fig. 4. Translational errors of the followers with switched δ_{iT}.

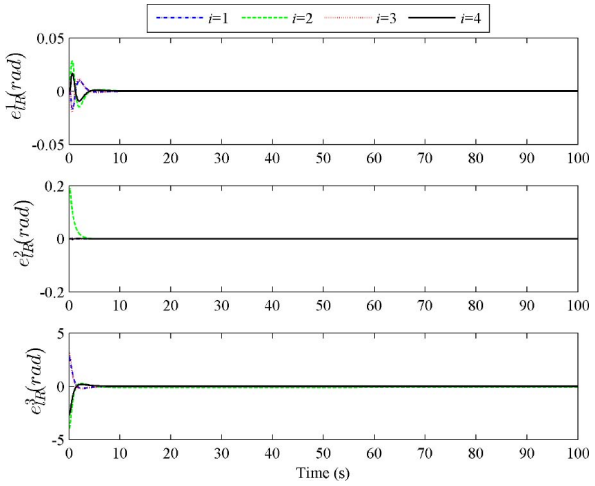

Fig. 5. Rotational errors of the leaders.

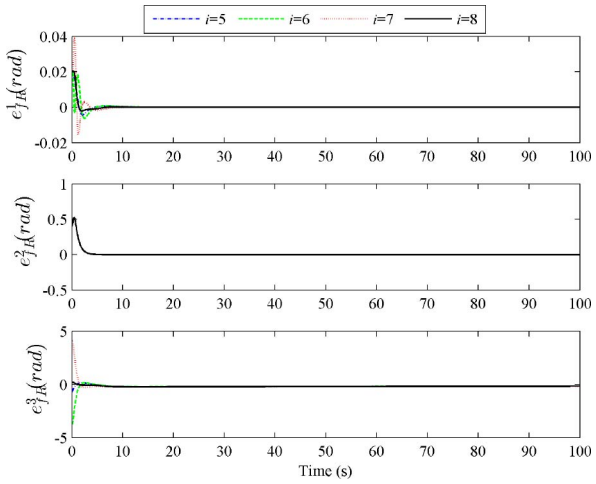

Fig. 6. Rotational errors of the followers.

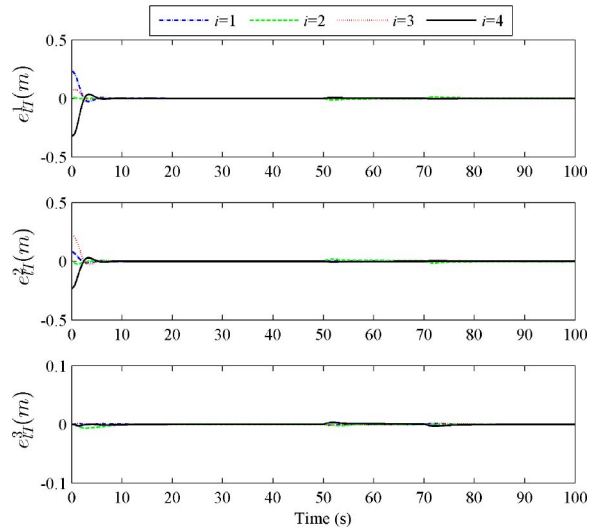

Fig. 7. Rotational errors of the leaders with time-varying δ_{iT}.

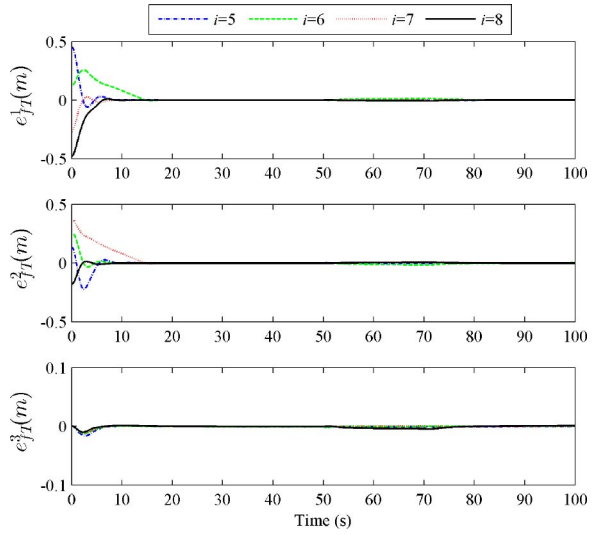

Fig. 8. Rotational errors of the followers with time-varying δ_{iT}.

it can also be designed for a configuration switch. In Figs. 3 and 4, $\boldsymbol{\delta}_{ij}$ for the rotational motion switches in the half time, therefore the errors of the formation have step changes accordingly. $\boldsymbol{\delta}_{ij}$ is designed smoothly for the translational motion to avoid sudden change, and the error signals are quite stable during the process, as shown in Figs. 7 and 8.

The estimation error of attitude angles is illustrated in Fig. 9. Given that the FWVs take off from the ground, their pitch

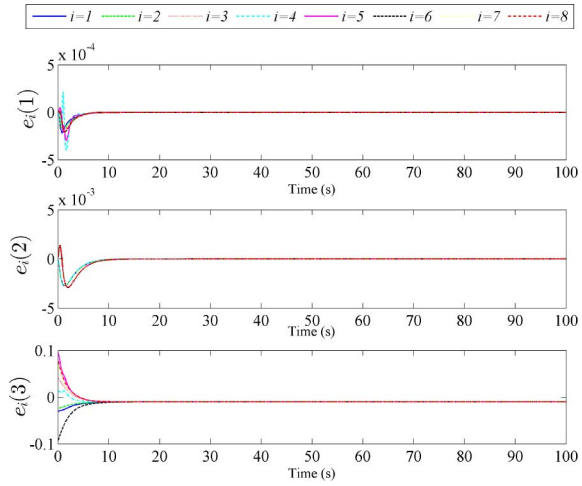

Fig. 9. Estimation errors of the attitude angles.

angles and roll angles are near zero. Their heading angles are set to be different initially. During flight, the FWVs estimate their attitude angles according to their translational tracking error. The estimated attitude angles converge to their true value in about 10 s. A small steady-state estimation error exists because the translational tracking error converges to zero, and no more correction can be made according to the translational tracking error. Similarly, rotational tracking also has a small steady-state error because of the estimation error. Nevertheless, the estimation error and the rotational tracking error are small enough (about 0.01 rad).

V. Conclusion

In this article, an attitude estimation and adaptive NN-based formation control method have been proposed for the FWV formation control problem. We first estimated the desired formation states according to communication typologies, then designed rotational and translational control algorithms for FWVs based on the NN technique and estimated attitude angles, and analyzed the stability of the control algorithms. Based on the observation that the translational states are coupled with the rotational states, an attitude estimation algorithm is proposed based on the coupling information. The convergence of the estimation algorithm is also analyzed. Finally, we conducted a series of simulations, which demonstrated the effectiveness of the proposed methods.

Appendix
Proof of Lemma 3

Matrix H_{IB} in (2) can be described by three matrices

$$H_\psi = \begin{bmatrix} \cos\psi & -\sin\psi & 0 \\ \sin\psi & \cos\psi & 0 \\ 0 & 0 & 1 \end{bmatrix}, \; H_\theta \begin{bmatrix} \cos\theta & 0 & \sin\theta \\ 0 & 1 & 0 \\ -\sin\theta & 0 & \cos\theta \end{bmatrix}$$
$$H_\phi = \begin{bmatrix} 1 & 0 & 0 \\ 0 & \cos\phi & -\sin\phi \\ 0 & \sin\phi & \cos\phi \end{bmatrix}. \tag{82}$$

Similarly

$$\bar{H}_\psi = \begin{bmatrix} \cos\bar{\psi} & -\sin\bar{\psi} & 0 \\ \sin\bar{\psi} & \cos\bar{\psi} & 0 \\ 0 & 0 & 1 \end{bmatrix}, \; \bar{H}_\theta \begin{bmatrix} \cos\bar{\theta} & 0 & \sin\bar{\theta} \\ 0 & 1 & 0 \\ -\sin\bar{\theta} & 0 & \cos\bar{\theta} \end{bmatrix}$$
$$\bar{H}_\phi = \begin{bmatrix} 1 & 0 & 0 \\ 0 & \cos\bar{\phi} & -\sin\bar{\phi} \\ 0 & \sin\bar{\phi} & \cos\bar{\phi} \end{bmatrix}. \tag{83}$$

Denote the estimation error for each attitude angle as

$$\begin{aligned} \Delta\psi &= \bar{\psi} - \psi \\ \Delta\theta &= \bar{\theta} - \theta \\ \Delta\phi &= \bar{\phi} - \phi. \end{aligned} \tag{84}$$

The difference between (82) and (83) can be calculated as

$$\begin{aligned} \Delta H_\phi &= \bar{H}_\phi - H_\phi \\ &= \begin{bmatrix} 0 & 0 & 0 \\ 0 & \cos\bar{\phi} - \cos\phi & -\sin\bar{\phi} + \sin\phi \\ 0 & \sin\bar{\phi} - \sin\phi & \cos\bar{\phi} - \cos\phi \end{bmatrix} \\ \Delta H_\theta &= \bar{H}_\theta - H_\theta \\ &= \begin{bmatrix} \cos\bar{\theta} - \cos\theta & 0 & \sin\bar{\theta} - \sin\theta \\ 0 & 0 & 0 \\ -\sin\bar{\theta} + \sin\theta & 0 & \cos\bar{\theta} - \cos\theta \end{bmatrix} \\ \Delta H_\psi &= \bar{H}_\theta - H_\theta \\ &= \begin{bmatrix} \cos\bar{\psi} - \cos\psi & -\sin\bar{\psi} + \sin\psi & 0 \\ \sin\bar{\psi} - \sin\psi & \cos\bar{\psi} - \cos\psi & 0 \\ 0 & 0 & 0 \end{bmatrix}. \end{aligned} \tag{85}$$

Substituting (82) into H_{IB} and (83) into $\bar{H}_{IB}$, note that $\bar{H}_{IB}^{-1} = \bar{H}_{IB}^{\mathrm{T}}$, we have

$$\begin{aligned} & H_{IB}\bar{H}_{IB}^{-1} - I \\ &= H_\psi H_\theta H_\phi \bar{H}_\phi^{\mathrm{T}} \bar{H}_\theta^{\mathrm{T}} \bar{H}_\phi^{\mathrm{T}} - I \\ &= H_\psi H_\theta \left(I + H_\phi \Delta H_\phi^{\mathrm{T}} \right) \bar{H}_\theta^{\mathrm{T}} \bar{H}_\phi^{\mathrm{T}} - I \\ &= H_\psi \Delta H_\psi^{\mathrm{T}} + H_\psi H_\theta \Delta H_\theta^{\mathrm{T}} H_\psi^{\mathrm{T}} + H_\psi H_\theta H_\phi \Delta H_\phi^{\mathrm{T}} H_\theta^{\mathrm{T}} H_\psi^{\mathrm{T}}. \end{aligned} \tag{86}$$

$H_\psi \Delta H_\psi^{\mathrm{T}}$, $H_\theta \Delta H_\theta^{\mathrm{T}}$, and $H_\phi \Delta H_\phi^{\mathrm{T}}$ are as follows:

$$\begin{aligned} H_\phi \Delta H_\phi^{\mathrm{T}} &= \begin{bmatrix} 0 & 0 & 0 \\ 0 & \cos\Delta\phi - 1 & \sin\Delta\phi \\ 0 & -\sin\Delta\phi & \cos\Delta\phi - 1 \end{bmatrix} \\ &= \Pi_\phi^{\mathrm{diag}} + \Pi_\phi^{ss} \\ H_\theta \Delta H_\theta^{\mathrm{T}} &= \begin{bmatrix} \cos\Delta\theta - 1 & 0 & -\sin\Delta\theta \\ 0 & 0 & 0 \\ \sin\Delta\theta & 0 & \cos\Delta\theta - 1 \end{bmatrix} \\ &= \Pi_\theta^{\mathrm{diag}} + \Pi_\theta^{ss} \\ H_\psi \Delta H_\psi^{\mathrm{T}} &= \begin{bmatrix} \cos\Delta\psi - 1 & \sin\Delta\psi & 0 \\ -\sin\Delta\psi & \cos\Delta\psi - 1 & 0 \\ 0 & 0 & 0 \end{bmatrix} \\ &= \Pi_\psi^{\mathrm{diag}} + \Pi_\psi^{ss} \end{aligned} \tag{87}$$

where Π_ψ^{diag}, $\Pi_\theta^{\mathrm{diag}}$, and Π_ϕ^{diag} are the diagonal matrices for ψ, θ, and ϕ, respectively, Π_ψ^{ss}, Π_θ^{ss}, and Π_ϕ^{ss}

are the corresponding skew-symmetric matrices. Then, we have

$$\begin{aligned}&\boldsymbol{x}^{\mathrm{T}}\Big(H_{IB}\bar{H}_{IB}^{-1}-I\Big)\boldsymbol{x}\\&=\boldsymbol{x}^{\mathrm{T}}\Big(\Pi_{\psi}^{\mathrm{diag}}+H_{\psi}\Pi_{\theta}^{\mathrm{diag}}H_{\psi}^{\mathrm{T}}+H_{\psi}H_{\theta}\Pi_{\phi}^{\mathrm{diag}}H_{\theta}^{\mathrm{T}}H_{\psi}^{\mathrm{T}}\Big)\boldsymbol{x}\\&\quad+\boldsymbol{x}^{\mathrm{T}}\Big(\Pi_{\psi}^{ss}+H_{\psi}\Pi_{\theta}^{ss}H_{\psi}^{\mathrm{T}}+H_{\psi}H_{\theta}\Pi_{\phi}^{ss}H_{\theta}^{\mathrm{T}}H_{\psi}^{\mathrm{T}}\Big)\boldsymbol{x}.\end{aligned}\tag{88}$$

Note that $H_{\psi}\Pi_{\theta}^{ss}H_{\psi}^{\mathrm{T}}$ and $H_{\psi}H_{\theta}\Pi_{\phi}^{ss}H_{\theta}^{\mathrm{T}}H_{\psi}^{\mathrm{T}}$ are also skew symmetric

$$\boldsymbol{x}^{\mathrm{T}}\Big(\Pi_{\psi}^{ss}+H_{\psi}\Pi_{\theta}^{ss}H_{\psi}^{\mathrm{T}}+H_{\psi}H_{\theta}\Pi_{\phi}^{ss}H_{\theta}^{\mathrm{T}}H_{\psi}^{\mathrm{T}}\Big)\boldsymbol{x}=0.\tag{89}$$

Since $H_{\psi}H_{\psi}^{\mathrm{T}}=I$ and $H_{\theta}H_{\theta}^{\mathrm{T}}=I$

$$\begin{aligned}&\boldsymbol{x}^{\mathrm{T}}\Big(\Pi_{\psi}^{\mathrm{diag}}+H_{\psi}\Pi_{\theta}^{\mathrm{diag}}H_{\psi}^{\mathrm{T}}+H_{\psi}H_{\theta}\Pi_{\phi}^{\mathrm{diag}}H_{\theta}^{\mathrm{T}}H_{\psi}^{\mathrm{T}}\Big)\boldsymbol{x}\\&=\boldsymbol{x}^{\mathrm{T}}\Pi_{\psi}^{\mathrm{diag}}\boldsymbol{x}+\boldsymbol{x}^{\mathrm{T}}\Pi_{\theta}^{\mathrm{diag}}\boldsymbol{x}+\boldsymbol{x}^{\mathrm{T}}\Pi_{\phi}^{\mathrm{diag}}\boldsymbol{x}\\&=\boldsymbol{x}^{\mathrm{T}}\Big(\Pi_{\psi}^{\mathrm{diag}}+\Pi_{\theta}^{\mathrm{diag}}+\Pi_{\phi}^{\mathrm{diag}}\Big)\boldsymbol{x}.\end{aligned}\tag{90}$$

The range of cosine function is $[-1, 1]$, and

$$\begin{aligned}\Pi_{H}^{rmdiag}&=\Pi_{\psi}^{\mathrm{diag}}+\Pi_{\theta}^{\mathrm{diag}}+\Pi_{\phi}^{\mathrm{diag}}\\&=\mathrm{diag}(\cos\Delta\psi+\cos\Delta\theta-2\\&\qquad\cos\Delta\phi+\cos\Delta\psi-2\\&\qquad\cos\Delta\phi+\cos\Delta\theta-2)\end{aligned}\tag{91}$$

which has no positive eigenvalue. Combining (88), (89), and (91), we have

$$\begin{aligned}&\boldsymbol{x}^{\mathrm{T}}\Big(H_{IB}\bar{H}_{IB}^{-1}-I\Big)\boldsymbol{x}\\&=\boldsymbol{x}^{\mathrm{T}}\Big(\Pi_{\psi}^{\mathrm{diag}}+H_{\psi}\Pi_{\theta}^{\mathrm{diag}}H_{\psi}^{\mathrm{T}}+H_{\psi}H_{\theta}\Pi_{\phi}^{\mathrm{diag}}H_{\theta}^{\mathrm{T}}H_{\psi}^{\mathrm{T}}\Big)\boldsymbol{x}\le 0.\end{aligned}\tag{92}$$

Therefore, $\boldsymbol{x}^{\mathrm{T}}(H_{IB}\bar{H}_{IB}^{-1}-I)\boldsymbol{x}\le 0$ always holds, and $\boldsymbol{x}^{\mathrm{T}}(H_{IB}\bar{H}_{IB}^{-1}-I)\boldsymbol{x}=0$ exists only if $\boldsymbol{x}=0$ or

$$\begin{aligned}\cos\Delta\psi+\cos\Delta\theta&=2\\\cos\Delta\phi+\cos\Delta\psi&=2\\\cos\Delta\phi+\cos\Delta\theta&=2\end{aligned}\tag{93}$$

which means $\Delta\psi=0$, $\Delta\theta=0$, and $\Delta\phi=0$, namely, $\bar{\boldsymbol{q}}_R=\boldsymbol{q}_R$. Thus, completes the proof of the first item.

The second item is quite straight forward. As analyzed above, the matrix $H_{IB}\bar{H}_{IB}^{-1}-I$ can be written as the sum of a diagonal matrix Π_{H}^{diag} and a skew-symmetric matrix Π_{H}^{ss}

$$H_{IB}\bar{H}_{IB}^{-1}-I=\Pi_{H}^{\mathrm{diag}}+\Pi_{H}^{ss}\tag{94}$$

where Π_{H}^{diag} is presented in (91) and $\lambda_{\max}(\Pi_{H}^{\mathrm{diag}})=0$. Then

$$\boldsymbol{x}^{\mathrm{T}}\Pi_{H}^{\mathrm{diag}}\boldsymbol{y}\le\lambda_{\max}\Big(\Pi_{H}^{\mathrm{diag}}\Big)\boldsymbol{x}^{\mathrm{T}}\boldsymbol{y}=0.\tag{95}$$

For any matrix skew-symmetric matrix $P\in\mathbb{R}^{N\times N}$, vector $\boldsymbol{x}$ and $\boldsymbol{y}$

$$\begin{aligned}\boldsymbol{x}^{\mathrm{T}}P\boldsymbol{y}&=\sum_{i=1}^{N}\sum_{j=1}^{N}P(i,j)(\boldsymbol{x}(i)\boldsymbol{y}(j)-\boldsymbol{x}(j)\boldsymbol{y}(i))\\&=\sum_{i=1}^{N}\sum_{j=1}^{N}P(i,j)\frac{\boldsymbol{x}^2(i)+\boldsymbol{x}^2(j)+\boldsymbol{y}^2(i)+\boldsymbol{y}^2(j)}{2}\\&\le\max(P(i,j))\cdot\big(\boldsymbol{x}^{\mathrm{T}}\boldsymbol{x}+\boldsymbol{y}^{\mathrm{T}}\boldsymbol{y}\big)\end{aligned}\tag{96}$$

where $P(i,j)$ is the element in the ith row and the jth column of matrix P, and $\boldsymbol{x}(i)$ and $\boldsymbol{y}(i)$ are the ith element in vector $\boldsymbol{x}$ and $\boldsymbol{y}$, respectively.

Based on the observation of H_{IB}, every element in the skew-symmetric matrix Π_{H}^{ss} is the sum of product of the sine and cosine functions. Every element in Π_{H}^{ss} is bounded, therefore $\max(\Pi_{H}^{\mathrm{ss}}(i,j))$ has an upper bound. We define the upper bound of $\Pi_{H}^{\mathrm{ss}}(i,j)$ as ϵ_h

$$\begin{aligned}\boldsymbol{x}^{\mathrm{T}}\Big(H_{IB}\bar{H}_{IB}^{-1}-I\Big)\boldsymbol{y}&=\boldsymbol{x}^{\mathrm{T}}\Big(\Pi_{H}^{\mathrm{diag}}+\Pi_{H}^{ss}\Big)\boldsymbol{y}\\&=\boldsymbol{x}^{\mathrm{T}}\Pi_{H}^{ss}\boldsymbol{y}\\&\le\max\big(\Pi_{H}^{\mathrm{ss}}(i,j)\big)\big(\boldsymbol{x}^{\mathrm{T}}\boldsymbol{x}+\boldsymbol{y}^{\mathrm{T}}\boldsymbol{y}\big)\\&\le\epsilon_h\big(\boldsymbol{x}^{\mathrm{T}}\boldsymbol{x}+\boldsymbol{y}^{\mathrm{T}}\boldsymbol{y}\big)\end{aligned}\tag{97}$$

thus complete the proof of item 2.

REFERENCES

[1] D. Mackenzie, "Avionics. A flapping of wings," *Science*, vol. 335, no. 6075, pp. 1430–1433, 2012.

[2] J. D. DeLaurier and J. M. Harris, "A study of mechanical flapping-wing flight," *Aeronaut. J.*, vol. 97, no. 968, pp. 277–286, 1993.

[3] J. D. DeLaurier, "An aerodynamic model for flapping-wing flight," *Aeronaut. J.*, vol. 97, no. 964, pp. 125–130, 1993.

[4] S. Ho, H. Nassef, N. Pornsinsirirak, Y.-C. Tai, and C.-M. Ho, "Unsteady aerodynamics and flow control for flapping wing flyers." *Progr. Aerosp. Sci.*, vol. 39, no. 8, pp. 635–681, 2003.

[5] S. P. Sane, and M. H. Dickinson, "The control of flight force by a flapping wing: Lift and drag production." *J. Exp. Biol.*, vol. 204, no. 15, pp. 2607–2626, 2001.

[6] M. Keennon, K. Klingebiel, and H. Won, "Development of the nano hummingbird: A tailless flapping wing micro air vehicle," in *Proc. 50th AIAA Aerosp. Sci. Meeting*, 2012, p. 1.

[7] A. Banazadeh and N. Taymourtash, "Adaptive attitude and position control of an insect-LKIE flapping wing air vehicle" *Nonlinear Dyn.*, vol.85, no. 1, pp. 47–66, 2012.

[8] W. He, Z. C. Yan, C. G. Sun, and Y. Chen, "Adaptive neural network control of a flapping wing micro aerial vehicle with disturbance observer," *IEEE Trans. Cybern.*, vol. 47, no. 10, pp. 3452–3465, Oct. 2017.

[9] P. Chirarattananon, Y. Chen, E. F. Helbling, K. Y. Ma, R. Cheng, and R. J. Wood, "Dynamics and flight control of a flapping-wing robotic insect in the presence of wind gusts," *Interface Focus*, vol. 7, no. 1, pp. 1–14, 2017.

[10] K. K. Oh, M. C. Park, and H. S. Ahn, "A survey of multi-agent formation control," *Automatica*, vol. 53, pp. 424–440, Mar. 2015.

[11] D. Li, S. S. Ge, W. He, G. Ma, and L. Xie, "Multilayer formation control of multi agent systems," *Automatica*, vol. 109, Nov. 2019, Art. no. 108558.

[12] Y. Q. Chen and Z. Wang, "Formation control: A review and a new consideration," in *Proc. IEEE/RSJ Int. Conf. Intell. Robots Syst.*, 2005, pp. 3181–3186.

[13] L Ma, Z Wang, and Q. L. Han, "Consensus control of stochastic multi-agent systems: A survey," *Sci. China Inf. Sci.*, vol. 12, pp. 5–19, Nov. 2017.

[14] B. Zhou and Z. L. Lin, "Consensus of high-order multi-agent systems with large input and communication delays," *Automatica*, vol. 50, no. 2, pp. 452–464, 2014.

[15] Y. Cao and W. Ren, "Containment control with multiple stationary or dynamic leaders under a directed interaction graph," in *Proc. IEEE Conf. Decis. Control*, 2009, pp. 3014–3019.

[16] H. Liu, L. Cheng, M. Tan, and Z.-G. Hou, "Containment control of continuous-time linear multi-agent systems with aperiodic sampling," *Automatica*, vol. 57, pp. 78–84, Jul. 2015.

[17] X. W. Dong, Y. Zhou, Z. Ren, and Y. Zhong, "Time-varying formation tracking for second-order multi-agent systems subjected to switching topologies with application to quadrotor formation flying," *IEEE Trans. Ind. Electron.*, vol. 64, no. 6, pp. 5014–5024, Jun. 2017.
[18] D. Lee, "Nonlinear disturbance observer-based robust control for spacecraft formation flying," *Aerosp. Sci. Technol.*, vol. 76, pp. 82–90, May 2018.
[19] Q. Hu, J. Zhang, and Y. Zhang, "Velocity-free attitude coordinated tracking control for spacecraft formation flying," *ISA Trans.*, vol. 53, pp. 54–65, Feb. 2018.
[20] L. Zhao and Y. Jia, "Neural network-based distributed adaptive attitude synchronization control of spacecraft formation under modified fast terminal sliding mode," *Neurocomputing*, vol. 171, pp. 230–241, Jan. 2016.
[21] D. Li, G. Ma, C. Li, W. He, J. Mei, and S. S. Ge, "Distributed attitude coordinated control of multiple spacecraft with attitude constraints via state and output feedback," *IEEE Trans. Aerosp. Electron. Syst.*, vol. 54, no. 5, pp. 2233–2245, Oct. 2018.
[22] H. G. Tanner and D. K. Christodoulakis. "Decentralized cooperative control of heterogeneous vehicle groups," *Robot. Auton. Syst.*, vol. 55, no. 11, pp. 811–823, 2007.
[23] H. G. de Marina, Z. Sun, M. Bronz, and G. Hattenberger, "Circular formation control of fixed-wing UAVs with constant speeds." in *Proc. IEEE/RSJ Int. Conf. Intell. Robots Syst. (IROS)*, 2017, pp. 5298–5303.
[24] A. Kalra, S. Anavatti, and R. Padhi, "Aggressive formation flying of fixed-wing UAVs with differential geometric guidance," *Unmanned Syst.*, vol. 5, no. 2, pp. 97–113, 2017.
[25] S. Y. Zhao, "Affine formation maneuver control of multi-agent systems," *IEEE Trans. Autom. Control*, vol. 63, no. 12, pp. 4140–4155, Dec. 2018.
[26] K. Fathian, T. H. Summers, and N. R. Gans, "Distributed formation control and navigation of fixed-wing UAVs at constant altitude," in *Proc. Int. Conf. Unmanned Aircraft Syst. (ICUAS)*, 2018, pp. 300–307.
[27] X. W. Liang, H. S. Wang, Y.-H. Liu, W. Chen, and T. Liu, "Formation control of nonholonomic mobile robots without position and velocity measurements," *IEEE Trans. Robot.*, vol. 34, no. 2, pp. 434–446, Apr. 2018.
[28] Z. Sun, H. G. de Marina, G. S. Seyboth, B. D. O. Anderson, and C. Yu, "Circular formation control of multiple unicycle-type agents with non-identical constant speeds," *IEEE Trans. Control Syst. Technol.*, vol. 27, no. 1, pp. 192–205, Jan. 2019.
[29] D. Dovrat and A. M. Bruckstein, "On gathering and control of unicycle agents with crude sensing capabilities," *IEEE Intell. Syst.*, vol. 32, no. 6, pp. 40–46, Apr. 2017.
[30] R. Wang and J. Liu, "Adaptive formation control of quadrotor unmanned aerial vehicles with bounded control thrust," *Chin. J. Aeronaut.*, vol. 30, no. 2, pp. 807–817, 2017.
[31] R. Sun, J. Wang, D. Zhang, Q. Jia, and X. Shao, "Roto-translational spacecraft formation control using aerodynamic forces," *J. Guid. Control Dyn.*, vol. 40, no. 10, pp. 1–24, 2017, doi: 10.2514/1.G003130
[32] M. Pastorelli, R. Bevilacqua, and S. Pastorelli, "Differential-drag-based Roto-translational control for propellant-less spacecraft," *Acta Astronautica*, vol. 114, pp. 6–21, Sep./Oct. 2015.
[33] M. M. Morrison, "Inertial measurement unit," U.S. Patent 4 711 125, Dec. 8, 1987.
[34] W. T. Fong, S. K. Ong, and A. Y. C. Nee, "Methods for in-field user calibration of an inertial measurement unit without external equipment," *Meas. Sci. Technol.*, vol. 19, no. 8, 2008, Art. no. 085202.
[35] S. Ghapani, J. Mei, W. Ren, and Y. Song, "Fully distributed flocking with a moving leader for Lagrange networks with parametric uncertainties," *Automatica*, vol. 67, pp. 67–76, May 2016.
[36] A. R. Mehrabian and K. Khorasani, "Constrained distributed cooperative synchronization and reconfigurable control of heterogeneous networked Euler–Lagrange multi-agent systems," *Inf. Sci.*, vols. 370–371, no. 5, pp. 578–597, 2016.
[37] M. Chen and S. S. Ge, "Adaptive neural output feedback control of uncertain nonlinear systems with unknown hysteresis using disturbance observer," *IEEE Trans. Ind. Electron.*, vol. 62, no. 12, pp. 7706–7716, Dec. 2015.
[38] F. Wang, B. Chen, C. Lin, J. Zhang, and X. Meng, "Adaptive neural network finite-time output feedback control of quantized nonlinear systems," *IEEE Trans. Cybern.*, vol. 48, no. 6, pp. 1839–1848, Jun. 2018.
[39] Y.-J. Liu, M. Gong, S. Tong, C. L. P. Chen, and D.-J. Li, "Adaptive fuzzy output feedback control for a class of nonlinear systems with full state constraints," *IEEE Trans. Fuzzy Syst.*, vol. 26, no. 5, pp. 2607–2617, Oct. 2018.
[40] J. Yang, J. Sun, W. X. Zheng, and S. Li, "Periodic event-triggered robust output feedback control for nonlinear uncertain systems with time-varying disturbance," *Automatica*, vol. 94, pp. 324–333, Aug. 2018.
[41] W. Xiao *et al.*, "Time-varying formation control for time-delayed multi-agent systems with general linear dynamics and switching topologies," *Unmanned Syst.*, vol. 7, no. 1, pp. 3–13, 2019.
[42] A. Soni and H. Hu, "Formation control for a fleet of autonomous ground vehicles: A survey," *Robotics*, vol. 7, no. 4, pp. 67, 2018.
[43] Z. Li, C.-Y. Su, L. Wang, Z. Chen, and T. Chai, "Nonlinear disturbance observer-based control design for a robotic exoskeleton incorporating fuzzy approximation," *IEEE Trans. Ind. Electron.*, vol. 62, no. 12, pp. 7706–7716, Sep. 2015.
[44] W. Ren and R. W. Beard, "Consensus seeking in multiagent systems under dynamically changing interaction topologies," *IEEE Trans. Autom. Control*, vol. 50, no. 5, pp. 655–661, May 2005.
[45] Z. Meng, W. Ren, and Z. You, "Distributed finite-time attitude containment control for multiple rigid bodies," *Automatica*, vol. 46, no. 12, pp. 2092–2099, 2010.
[46] D. Y. Li, W. Zhang, W. He, C. Li, and S. S. Ge, "Two-layer distributed formation-containment control of multiple Euler–Lagrange systems by output feedback," *IEEE Trans. Cybern.*, vol. 49, no. 2, pp. 675–687, Feb. 2019.
[47] S. S. Ge, T. H. Lee, and C. J. Harris, *Adaptive Neural Network Control of Robotic Manipulators*. Singapore: World Sci., 1998.
[48] M. Kubat, "Neural networks: A comprehensive foundation by Simon Haykin, Macmillan, 1994, ISBN 0-02-352781-7," *Knowl. Eng. Rev.*, vol. 13, no. 4, pp. 409–412, 1999.
[49] B. Xu and F. Sun, "Composite intelligent learning control of strict-feedback systems with disturbance," *IEEE Trans. Cybern.*, vol. 48, no. 2, pp. 730–741, Feb. 2018.
[50] S. S. Ge and C. Wang, "Adaptive neural control of uncertain MIMO nonlinear systems," *IEEE Trans. Neural Netw.*, vol. 15, no. 3, pp. 647–692, May 2004.